Electronic Supplementary Material (ESI) for Organic Chemistry Frontiers.

Sharing the salt bowl: Counterion identity drives *N*-alkyl resorcinarene affinity and selectivity for pyrophosphate in water

Kwaku Twum,[a] Seyed Iraj Sadraei,[b] Jordan Feder,[a] S. Maryamdokht Taimoory,*[b,c] Kari Rissanen,*[d] John F. Trant*[b] and Ngong Kodiah Beyeh*[a]

[a] *Oakland University, Department of Chemistry, 146 Library Drive, Rochester, MI 48309-4479, USA*
[b] *University of Windsor, Department of Chemistry and Biochemistry, Windsor, ON, N9B 3P4, Canada*
[c] *University of Michigan, Department of Chemistry, Ann Arbor, MI, USA*
[d] *University of Jyvaskyla, Department of Chemistry, P. O. Box 35, 40014 Jyvaskyla, Finland.*

SUPPORTING INFORMATION

Table of Contents

1. GENERAL INFORMATION

The *N*-alkyl ammonium resorcinarene salts (NARYs) were synthesized according to reported procedures.[1–4] The reagents for synthesis and the phosphates (K_3PO_4, Na_4PPi, Na_2AMP, Na_2ADP, and Na_2ATP) were purchased from commercial sources and used without purification. The synthesis of C3OHNARCl, CyNARCl, and BnNARCl are reported elsewhere.[1] ^1H, ^{13}C and ^{31}P NMR spectra were recorded on a Bruker Avance DRX 400 (400 MHz for ^1H, 100 MHz for ^{13}C and 161.89 MHz for ^{31}P) spectrometer. All signals are given as δ values in ppm using residual solvent signals as the internal standard. Coupling constants are given in Hz. Melting points were determined with a Stuart capillary melting point apparatus. Experimental details for the synthesis and characterization data of C3OHNARBr, C3OHNAROTf, CyNARBr, BnNARBr, NpNARCl, NpNARBr and NpNAROTf are below.

2. SYNTHESIS

The resorcinarene **1** and the hydroxyl tetrabenzoxazine **2** were synthesized by reported procedure.[1]

a. General procedure for the synthesis of tetrabenzoxazines from the resorcinarenes. To a solution of the resorcinarene (5.5 mmol) and excess formaldehyde (6 mL) in ethanol (40 mL) was added the amine (23.3 mmol) in ethanol (15 mL) slowly and stirred at room temperature for 24 h. The precipitate that separated was filtered, recrystallized in a methanol/n-hexane mixture and used in the next step without any further purification.

b. General procedure for the synthesis of the *N*-alkyl ammonium resorcinarene chlorides from the tetrabenzoxazines. A solution of the tetrabenzoxazine (0.92 mmol), 3 mL of concentrated acid and 4 mL of H_2O in 40 mL of isopropanol is heated under reflux. Water and formaldehyde were removed by azeotropic distillation with chloroform. The remaining isopropanol was evaporated, and the crude product triturated with diethyl ether. The product was recrystallized accordingly to yield the pure product.

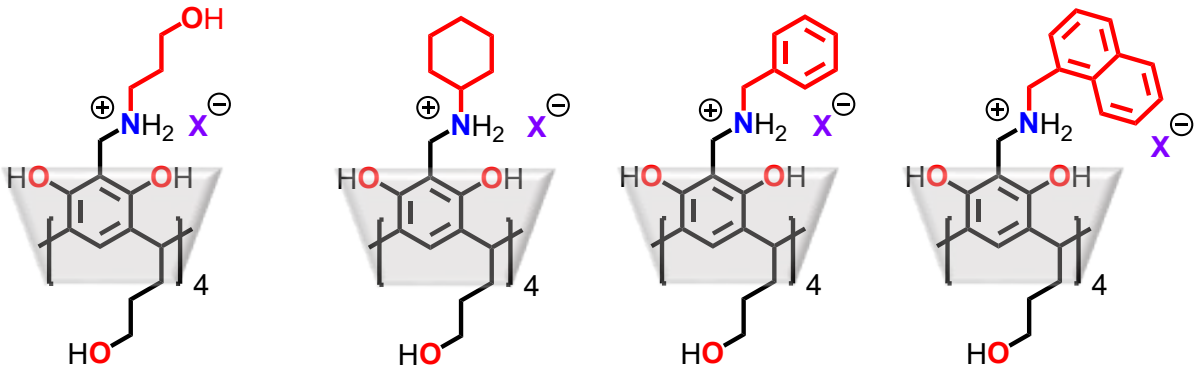

X = Cl,	C3OHNAR(Cl)$_4$	CyNAR(Cl)$_4$	BnNAR(Cl)$_4$	NpNAR(Cl)$_4$
X = Br,	C3OHNAR(Br)$_4$	CyNAR(Br)$_4$	BnNAR(Br)$_4$	NpNAR(Br)$_4$
X = CF_3SO_3,	C3OHNAR(OTf)$_4$			NpNAR(OTf)$_4$

Figure S1. General representation of *N*-alkyl ammonium resorcinarene salts, R-NARX$_4$.

2.1 Synthetic details of *N*-propanol ammonium resorcinarene bromide, C3OHNARBr$_4$

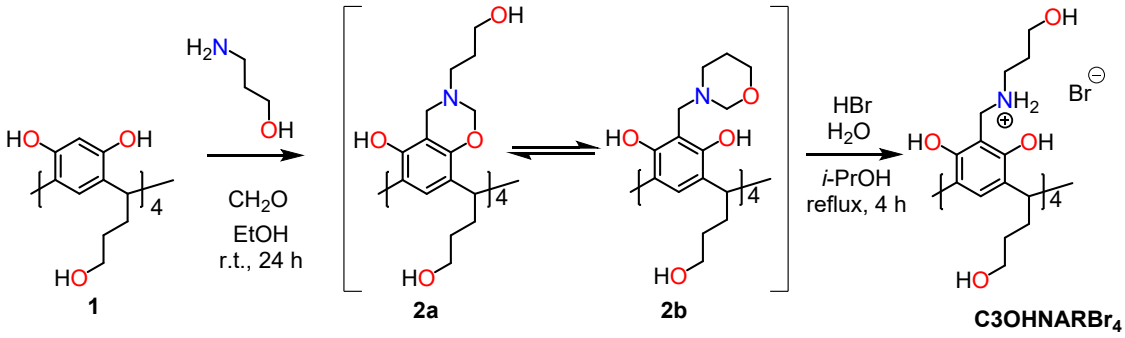

Figure S2. Synthesis of *N*-propanol ammonium resorcinarene bromide, C3OHNARBr$_4$.

The tetrabenzoxazine **2** (1.0 g, 0.92 mmol), isopropanol (40 ml), hydrobromic acid (3 ml), and H_2O (4 ml). The crude product mixture was recrystallized in a 1:1 (v/v) mixture of tetrahydrofuran and diethyl ether. The resulting precipitate was washed with acetonitrile, THF, Diethyl ether, and dried (393.7 mg, 30.2% yield). Melting point > 300°C. ESI-TOF-HRMS (Positive ion mode, sprayed from MeOH): m/z found 361.86320 $[M\text{-}4Br\text{-}1H]^{+3}$; calc. 361.8752, m/z found 582.25461$[M\text{-}3Br\text{-}1H]^{+2}$; calc. 582.2723. ^{1}H NMR (400 MHz in D_2O/[D_6]DMSO 9/1 v/v, 298 K) δ (ppm): 1.50 (m, 8H,CH_2), 2.33 (m, 8H,CH_2), 3.13 (t, J = 5.27 Hz, 8H, CH_2),3.30 (m, 8H, CH_2), 3.65(t, J = 6.52 Hz, 8H, CH_2), 3.81 (q, J = 5.70 Hz, 8H, CH_2), 4.28 (t, J = 7.64 Hz, 8H,CH_2), 4.45 (t, J = 7.97 Hz, 4H, CH), 7.49 (s, 4H, CH); ^{13}C NMR: (100 MHz, 298 K in CD_3OD) δ (ppm) = 29.9, 34.3, 41.2, 48.4, 56.3, 61.4, 81.7, 126.9, 150.4.

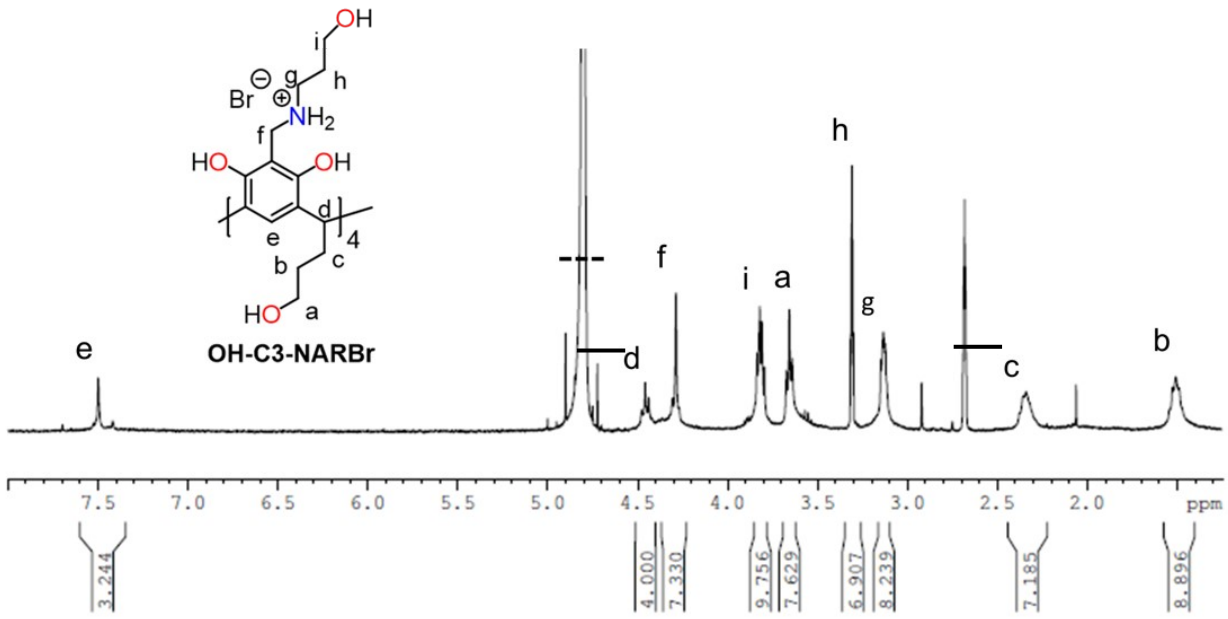

Figure S3. ^{1}H NMR of *N*-propanol ammonium resorcinarene bromide, C3OHNARBr$_4$, in D_2O/[D_6]DMSO 9/1, v/v at 298 K.

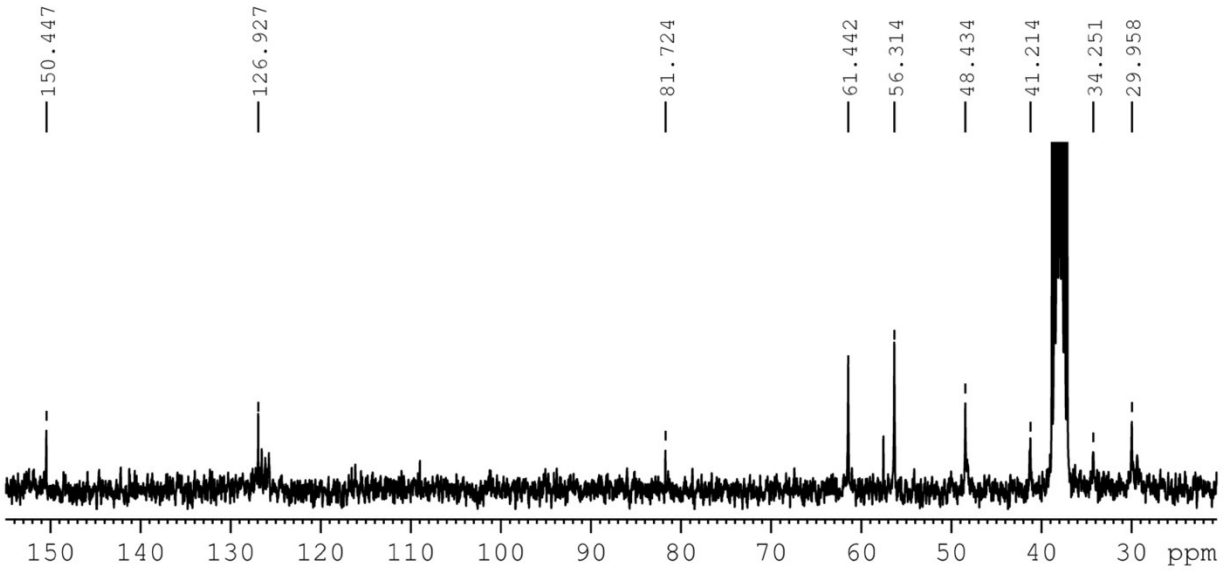

Figure S4. ^{13}C NMR of *N*-propanol ammonium resorcinarene bromide, C3OHNARBr$_4$, in [D$_6$]DMSO at 298 K.

2.2 Synthetic details of *N*-propanol ammonium resorcinarene triflate, C3OHNAROTf$_4$

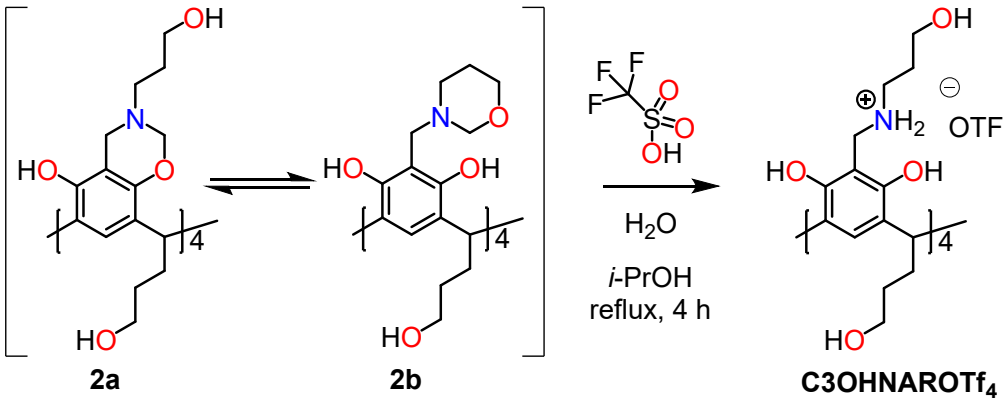

Figure S5. Synthesis of *N*-propanol ammonium resorcinarene triflate, C3OHNAROTf$_4$.

The tetrabenzoxazine **2** (1.0 g 0.92 mmol), isopropanol (40 ml), concentrated triflic acid (3 ml), and H_2O (4 ml). The precipitate was washed with ethyl acetate and then with diethyl ether (371.8 mg, 23.8 %). Melting points = 155-157^{o}C. ESI-TOF-HRMS (Positive ion mode, sprayed from MeOH): m/z found 271.64498 [M-4CF$_3$SO$_3$]$^{+4}$; calc. 271.6583, m/z found 617.27153 [M-3CF$_3$SO$_3$-1H]$^{+2}$, calc. 617.2891. ^{1}H NMR (400 MHz in D$_2$O) δ (ppm):1.43 (t, J = 5.99 Hz, 8H, CH$_2$), 1.74 (t, J = 5.99 Hz, 8H, CH$_2$) 2.19 (s, 8H, CH$_2$), 2.97, (t, J = 6.99 Hz, 8H,CH$_2$), 3.50 (t J = 5.99 Hz,8H,CH$_2$), 3.57 (t, J = 6.24 Hz, 8H, CH$_2$), 4.19(s, 8H, CH$_2$), 4.36 (t, J = 7.23 Hz, 4H, CH), 7.29 (s, 4H, CH); ^{13}C NMR: (100 MHz, 298 K in [D$_6$]DMSO) δ (ppm) = 21.1, 29.5, 31.3, 34.5, 41.4, 49.4, 56.6, 60.7, 108.6, 117.3, 119.8, 122.4, 125.0, 126.4, 150.87, 171.0.

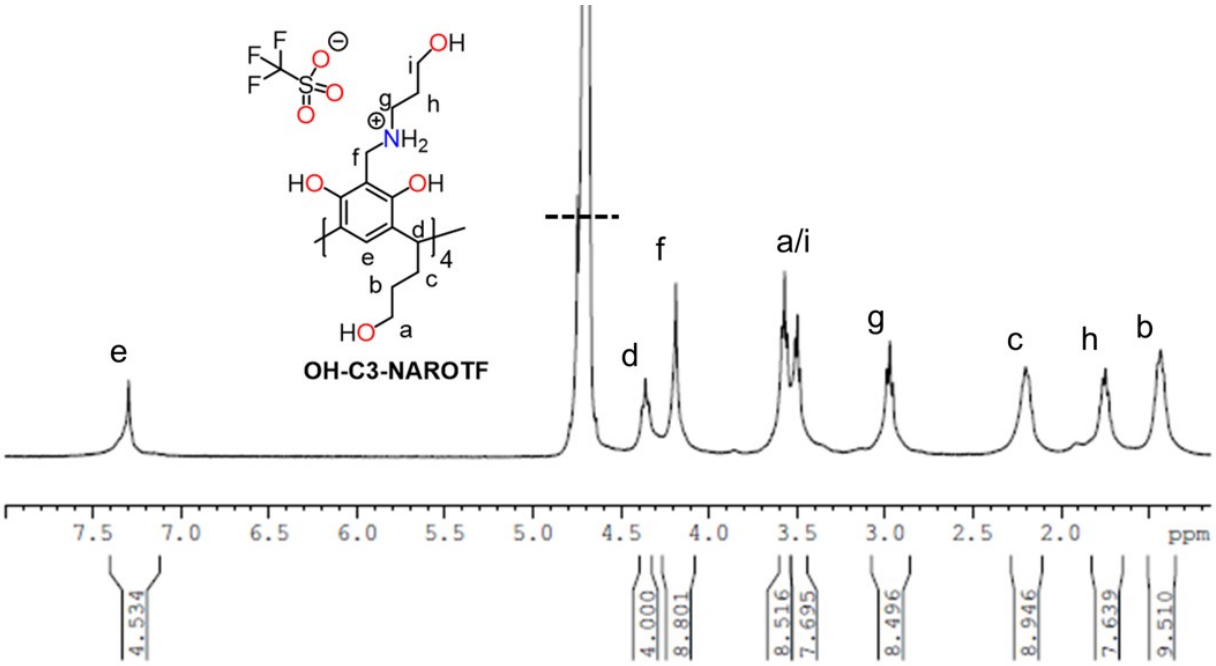

Figure S6. ^{1}H NMR of *N*-propanol ammonium resorcinarene triflate, C3OHNAROTf$_4$, in D_2O at 298 K.

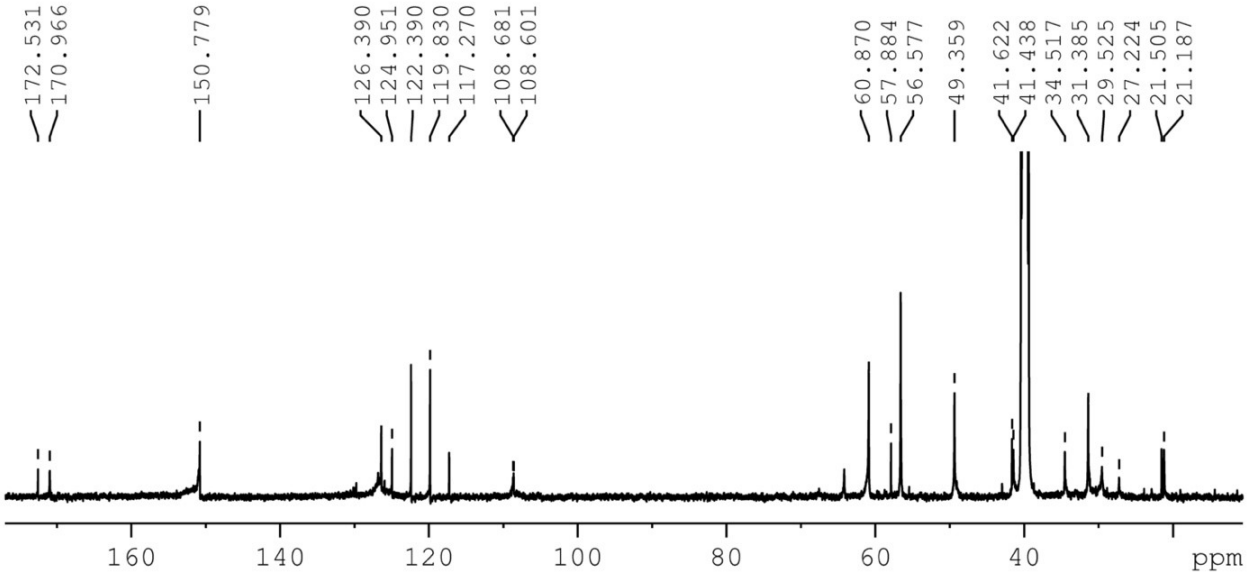

Figure S7. ^{13}C NMR of *N*-propanol ammonium resorcinarene triflate, C3OHNAROTf$_4$, in [D_6]DMSO at 298 K.

2.3 Synthetic details of *N*-cyclohexyl ammonium resorcinarene bromide, CyNARBr$_4$

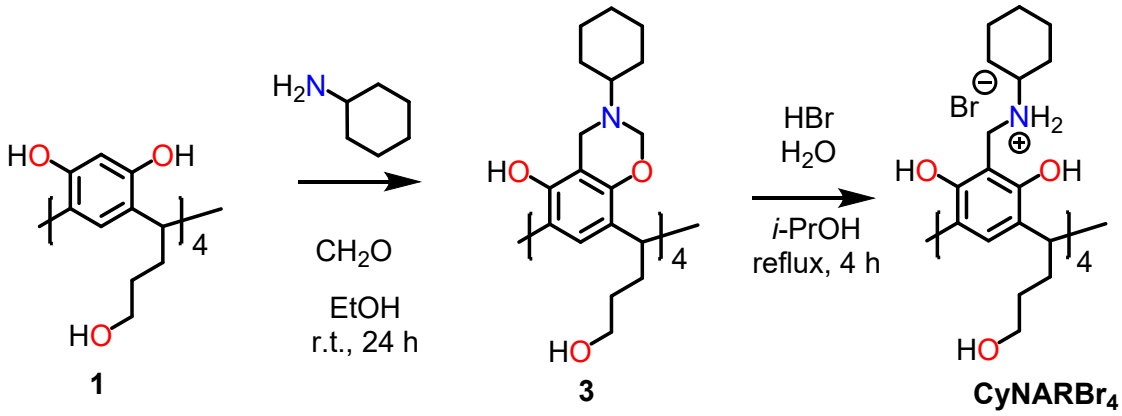

Figure S8. Synthesis of *N*-cyclohexyl ammonium resorcinarene bromide, CyNARBr$_4$.

Resorcinarene, **1** (5.0 g, 6.9 mmol) and excess formaldehyde solution 36 % (28 mL), ethanol (60 ml), cyclohexylamine (2.87 mL, 25.18 mmol) in ethanol (15 mL). The *N*-cyclohexyltetrabenzoxazine precipitate was filtered and dried and used in the next step without further purification. The *N*-cyclohexyltetrabenzoxazine **3** (1.0 g, 0.92 mmol), isopropanol (40 ml), concentrated hydrobromic acid (3 ml), and H_2O (4 ml). The precipitate was washed with ethyl acetate and then with diethyl ether to give the CyNARBr$_4$ product (371.8 mg, 23.8 % yield). Melting point > 300^{o}C. ESI-TOF-HRMS (Positive ion mode, sprayed from MeOH): m/z found 583.37324 $[M\text{-}4Br\text{-}2H]^{+2}$; calc. 583.3742, m/z found 623.33316 $[M\text{-}3Br\text{-}H]^{+2}$, calc. 623.3373. ^{1}H NMR (400 MHz in D_2O) δ (ppm): 0.9 (m, 12H, CH_2), 1.19 (m, 12H, CH_2), 1.53 (m, 12H, CH_2), 1.56 (d, J = 12.42 Hz, 8H, CH_2), 1.79 (d, J = 11.61 Hz, 8H, CH_2), 2.26 (q, J = 7.55 Hz, 8H, CH_2), 2.68 (m, 4H, CH), 3.60 (t, J = 6.47 Hz, 8H, CH_2), 4.19 (s, 8H, CH_2), 4.38 (t, J = 7.84 Hz, 4H, CH), 7.37 (s, 4H, ArH); ^{13}C NMR: (100 MHz, 298 K in D_2O) δ (ppm) = 14.0, 23.8, 24.2, 28.7, 29.5, 29.7, 34.2, 38.6, 56.5, 61.5, 65.9, 109.0, 125.3, 126.9, 150.1.

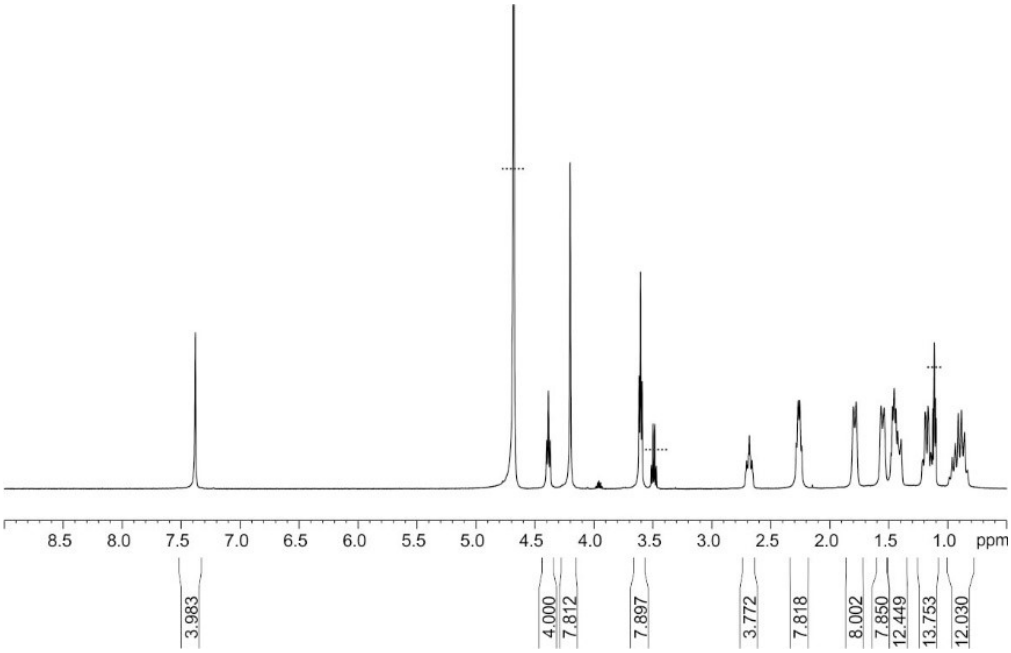

Figure S9:. ^{1}H NMR of *N*-cyclohexyl ammonium resorcinarene bromide, CyNARBr$_4$ in D_2O at 298 K.

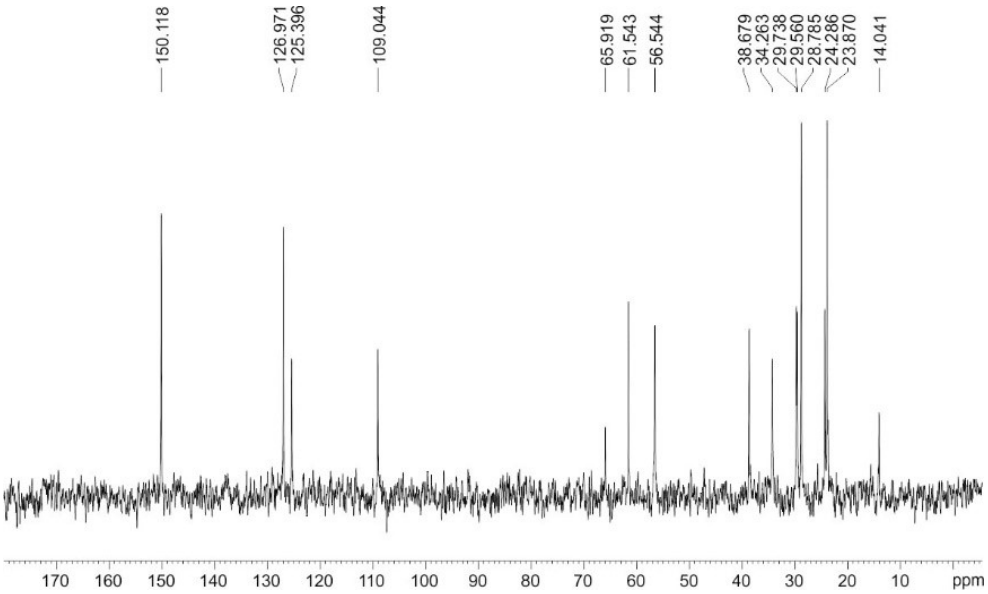

Figure S10. ^{13}C NMR of *N*-cyclohexyl ammonium resorcinarene bromide, CyNARBr$_4$ in D_2O at 298 K.

2.4 Synthetic details of *N*-benzyl ammonium resorcinarene bromide, BnNARBr$_4$

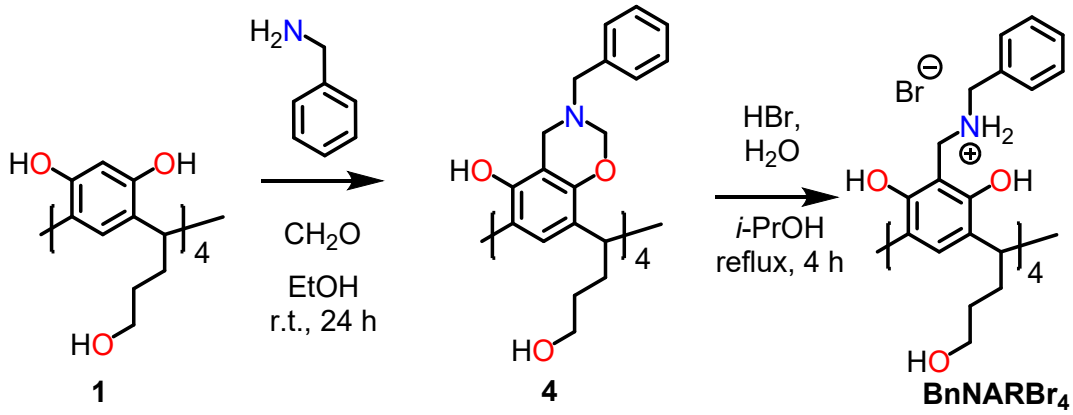

Figure S11. Synthesis of *N*-benzyl ammonium resorcinarene bromide, BnNARBr$_4$.

Resorcinarene, **1** (5.0 g, 6.9 mmol) and excess formaldehyde solution 36 % (28 mL), ethanol (60 ml), benzylamine (3.18 mL, 29.11 mmol) in ethanol (15 mL). The *N*-benzyl tetrabenzoxazine precipitate was filtered and dried and used in the next step without further purification. The *N*-benzyltetrabenzoxazine **4** (1.0 g 0.92 mmol), isopropanol (40 ml), concentrated hydrobromic acid (3 ml), and H_2O (4 ml). The precipitate was washed with ethyl acetate and then with diethyl ether to give the BnNARBr$_4$ product (371.8 mg, 23.8 %). Melting point > 250^{o}C, ESI-TOF-HRMS (Positive ion mode, sprayed from MeOH): m/z found 399.87685 $[M\text{-}4Br\text{-}1H]^{+3}$; calc. 399.8768, m/z found 1197.61758 $[M\text{-}4Br\text{-}3H]^{+}$; calc. 1197.6159. ^{1}H NMR (400 MHz in D_2O/$[D_6]$DMSO 9/1, δ (ppm): 1.51(m, 8H, CH_2), 2.36(q, J = 7.06 Hz, 8H,CH_2), 3.67 (t, J = 6.98 Hz, 8H, CH_2), 3.81 (s, 8H, CH_2), 4.28 (s, 8H,

CH_2), 4.30 (t, J = 4.42 Hz, 4H, CH), 6.75 (m, 20H, Ar), 7.58 (s, 4H, CH); ^{13}C NMR: (100 MHz, 298 K in CD_3OD) δ (ppm) = 30.4, 34.6, 42.7, 50.7, 56.5, 60.9, 108.9, 126.5, 129.1, 129.3, 129.5, 130.6, 132.0, 150.7,

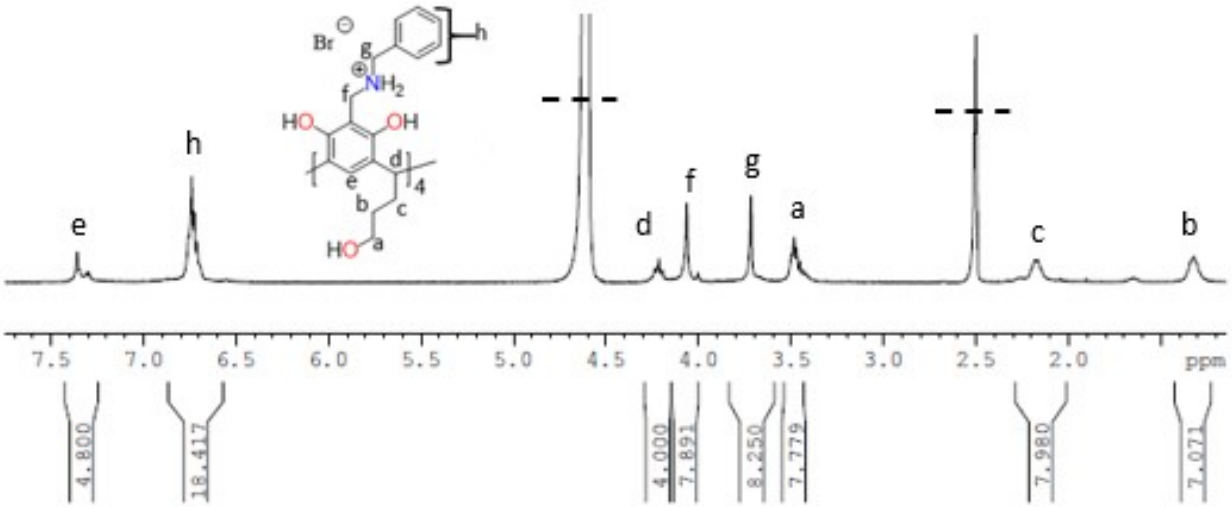

Figure S12. ^{1}H NMR of *N*-benzyl ammonium resorcinarene bromide, $BnNARBr_4$, in $D_2O/[D_6]DMSO$ 9/1, v/v at 298 K.

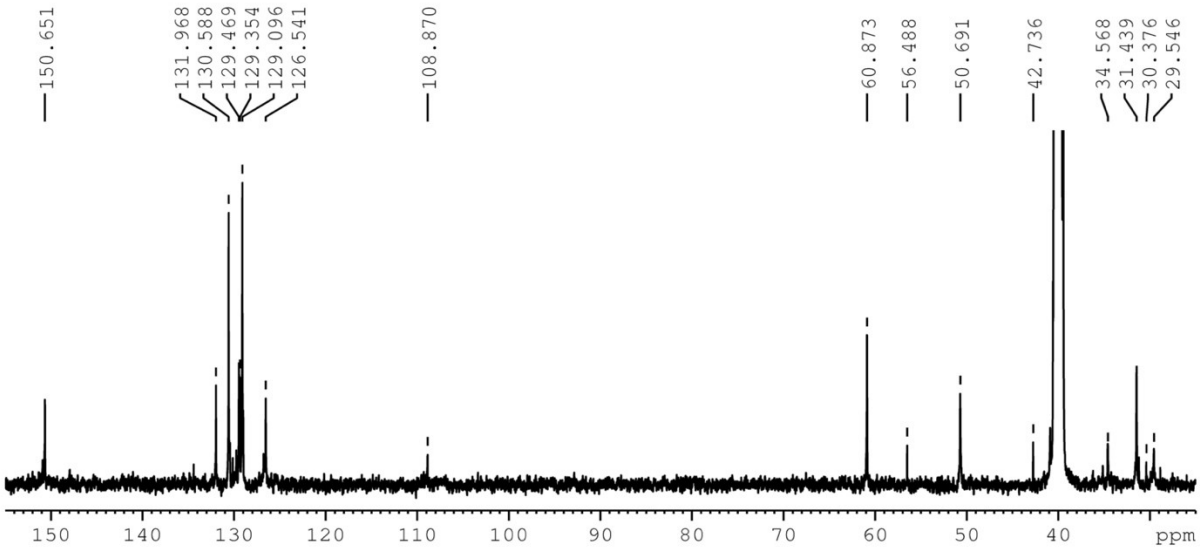

Figure S13. ^{13}C NMR of *N*-benzyl ammonium resorcinarene bromide, $BnNARBr_4$, in $[D_6]DMSO$ at 298 K.

2.5 Synthetic details of *N*-naphthyl ammonium resorcinarene chloride, $NpNARCl_4$

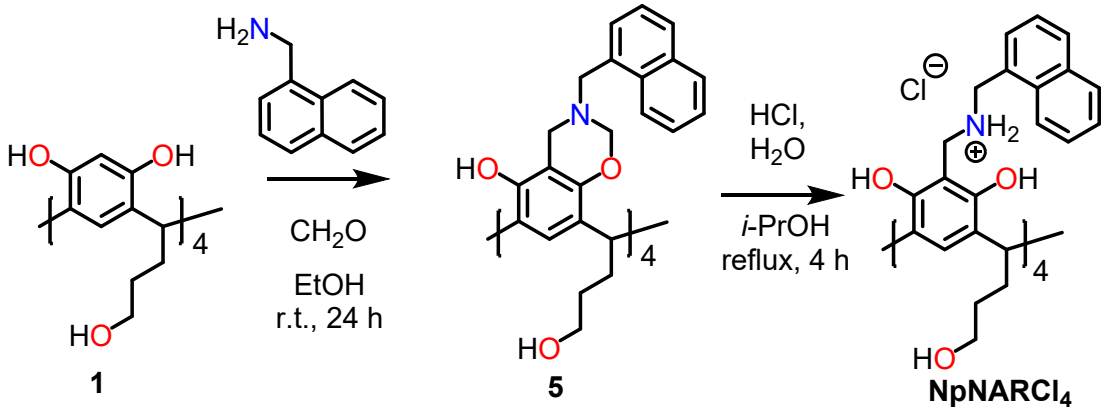

Figure S14. Synthesis of *N*-naphthyl ammonium resorcinarene chloride, $NpNARCl_4$.

Resorcinarene, **1** (5.0 g, 6.9 mmol) and excess formaldehyde solution 36 % (28 mL), ethanol (60 ml), 1-napthylmethylamine (4.25 mL, 29 mmol) in ethanol (15 mL). The precipitate was filtered and dried and used in the next step without further purification. The naphthyltetrabenzoxazine, **5** (0.5 g, 0.36 mmol), isopropanol (25 mL), 1.5 mL concentrated HCl (37 %), 2 mL H_2O.The crude product was then recrystallized with methanol and then triturated in diethyl ether to give the $NpNARCl_4$ product (0.23 g, 42 % yield). Melting points > 300°C. ESI-TOF-HRMS (Positive ion mode, sprayed from MeOH): *m/z* Found 699.34303 $[M-4Cl-2H]^{+2}$; calc. 699.3429, m/z found 1433.66197 $[M-3Cl-2H]^{+}$; calc. 1433.6551. ^1H NMR (400 MHz in $D_2O/[D_6]DMSO$ 9/1) δ(ppm): 1.56 (m, 8H, CH_2), 2.43 (q, J = 7.66 Hz, 8H, CH_2), 3.72 (t, J = 6.4 Hz, 8H, CH_2,), 3.85 (s, 8H, CH_2), 3.96 (s, 8H, CH_2), 4.41 (t, J = 8.21 Hz, 4H, CH) 6.60-7.7 (m, Ar, 32H): ^{13}C NMR: (400 MHz, 298 K in $D_2O/[D_6]DMSO$ 9/1) δ (ppm) = 30.9, 31.6, 35.9, 42.3, 47.2, 63.1, 110.4, 122.5, 126.6, 127.0, 127.3, 128.2, 129.1, 130.8, 131.7, 134.5, 151.6.

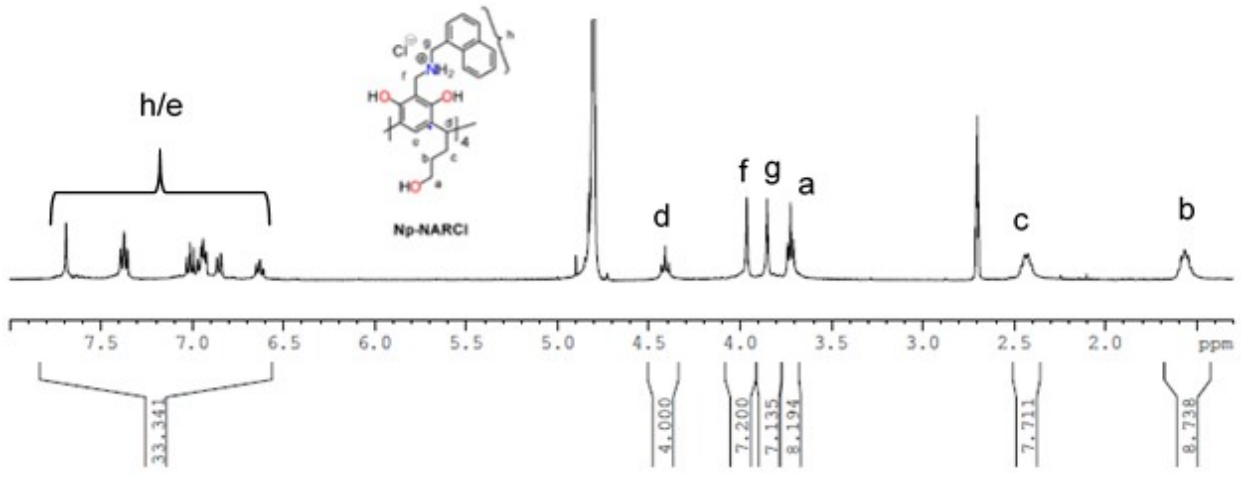

Figure S15. ^1H NMR of *N*-naphthyl ammonium resorcinarene chloride, $NpNARCl_4$, in $D_2O/[D_6]DMSO$ 9/1 v/v at 298 K.

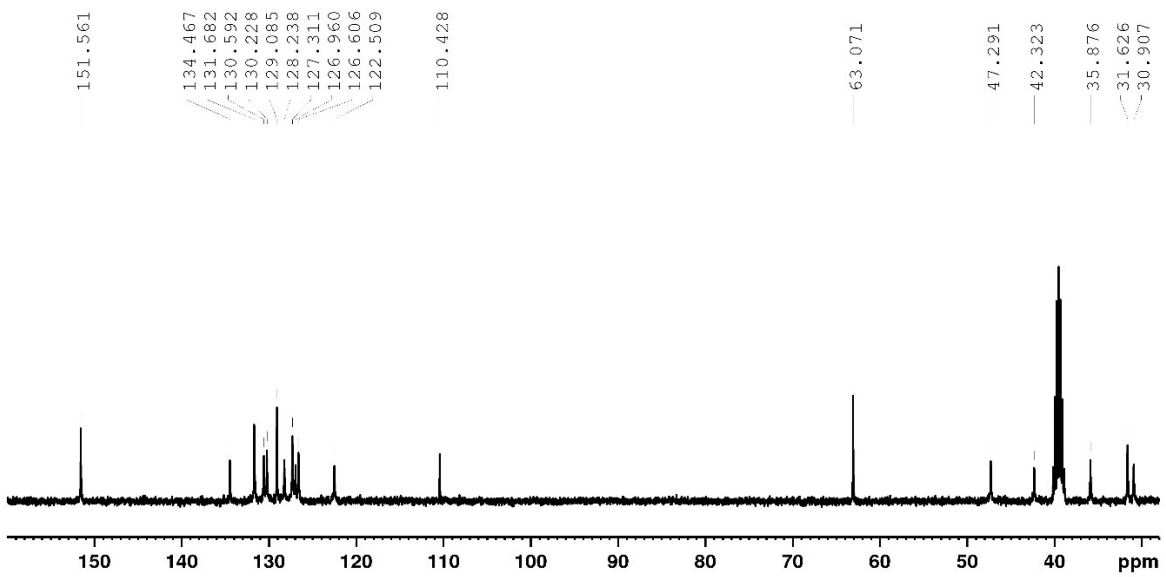

Figure S16. ^{13}C NMR of *N*-naphthyl ammonium resorcinarene chloride, NpNARCl$_4$, in D$_2$O/[D$_6$]DMSO 9/1 v/v at 298 K.

2.6 Synthetic details of *N*-naphthyl ammonium resorcinarene bromide, NpNARBr$_4$

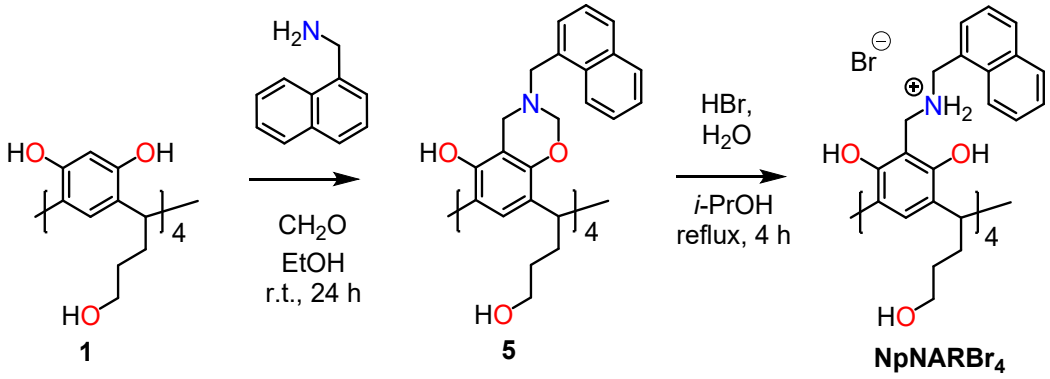

Figure S17. Synthesis of *N*-naphthyl ammonium resorcinarene bromide, NPNARBr

Naphthyl-tetrabenzoxazine (0.5 g .36 mmol), isopropanol (25 mL), 1.5 mL concentrated hydrobromic acid, 2 mL H$_2$O. The crude product was then recrystallized with methanol and then triturated in diethyl ether to give the NpNARBr product (0.14g, 28% yield). Melting point > 300 ^{o}C. ESI-TOF-HRMS (Positive ion mode, sprayed from MeOH): *m/z* Found 699.34361 [M-4Br-2H]$^{+2}$; calc. 699.3429, m/z found 466.56612 [M-4Br-1H]$^{+3}$; calc. 466.5643. ^{1}H NMR (400 MHz in D$_2$O/[D$_6$]DMSO 9/1, v/v), δ (ppm): 1.65 (m, H8, CH$_2$), 2.44 (q, J = 7.51 Hz, H8, CH$_2$), 7.72 (t, J = 6.41 Hz, 8H, CH$_2$), 3.87 (d, J = 6.33 Hz, 8H, CH$_2$), 6.96 (s, 8H, CH$_2$), 4.41 (m, 4H, CH), 6.63-7.74 (m, 32H, ArH); ^{13}C NMR: (100 MHz, 298 K in CD$_3$OD) δ (ppm) = 26.0, 31.5, 34.7, 41.6, 47.2, 61.0, 123.8, 125.8, 126.6, 126.7, 127.3, 128.1, 129.2, 129.7, 130.2, 131.7, 133.7, 150.7.

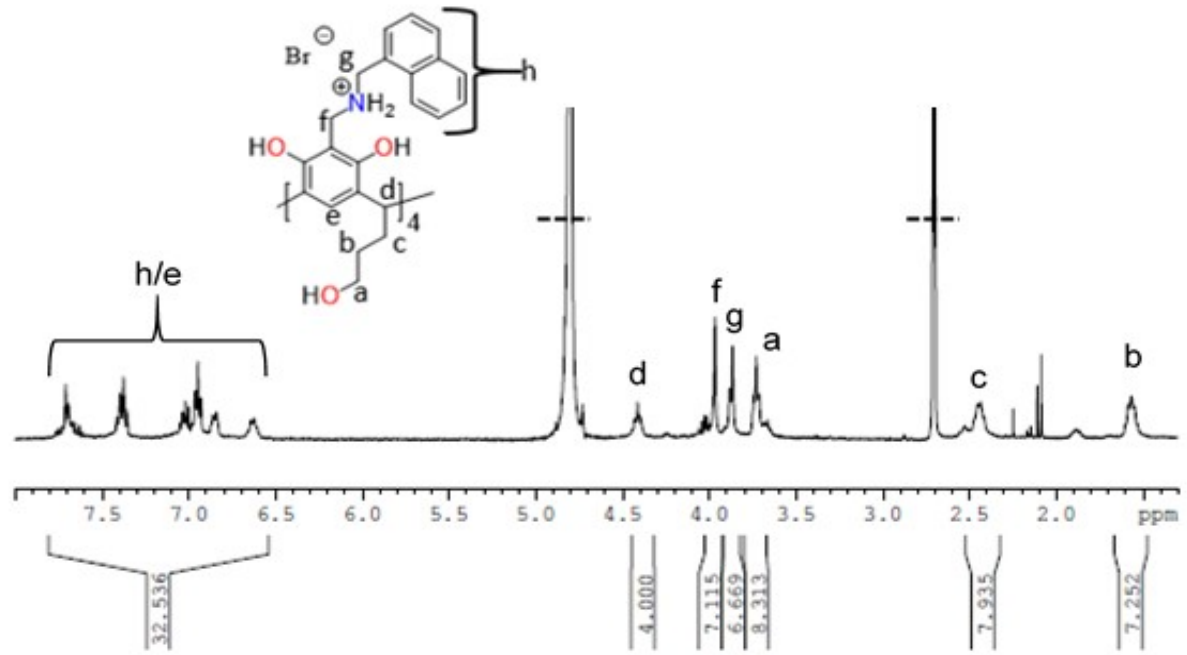

Figure S18. ^{1}H NMR of *N*-naphthyl ammonium resorcinarene bromide, NpNARBr$_4$, in D$_2$O/[D$_6$]DMSO 9/1, v/v at 298 K.

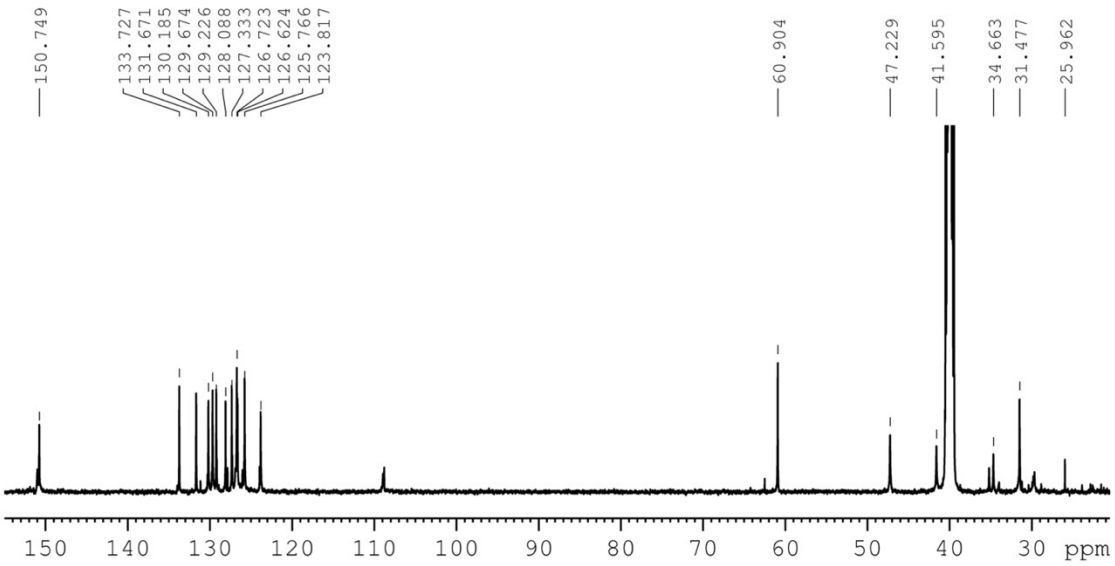

Figure S19. ^{13}C NMR of *N*-naphthyl ammonium resorcinarene bromide, NpNARBr$_4$, in [D$_6$]DMSO at 298 K.

2.7 Synthetic details of *N*-naphthyl ammonium resorcinarene triflate, NpNAROTf$_4$

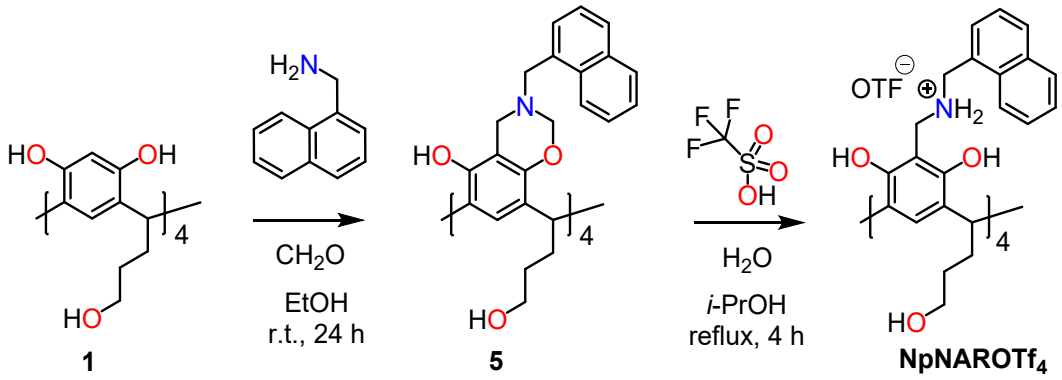

Figure S20. Synthesis of *N*-naphthyl ammonium resorcinarene triflate, NpNAROTf$_4$.

Naphthyl-tetrabenzoxazine (0.5 g .36 mmol), isopropanol (25 mL), 1.0 mL of triflic acid (99%) in 6 mL H_2O.The crude product was then recrystallized with methanol and then triturated in diethyl ether to give the NpNAROTf product (0.97g, 70 %). Melting point > 300 ^oC; ESI-TOF-HRMS (Positive ion mode, sprayed from MeOH): *m/z* found 699.34245 $[M\text{-}4CF_3SO_3\text{-}2H]^{+2}$; calc. 699.3429, m/z found 774.32331 $[M\text{-}3CF_3SO_3\text{-}H]^{+2}$, calc. 774.3228. ^1H NMR (400 MHz in D_2O) δ (ppm): 1.55 (m, 8H, CH_2), 2.41 (q, J = 7.63 Hz, 8H, CH_2), 3.71 (t, J = 6.43Hz, 8H, CH_2), 3.83 (s, 8H, CH_2), 3.96 (s, 8H, CH_2), 4.39 (t, J = 7.65 Hz, 4H, CH_1) 6.55-8.17 (m, 32H, Ar): ^{13}C NMR: (100 MHz, 298 K in CD_3OD) δ (ppm) = 22.5, 31.3, 35.4, 41.8, 46.8, 62.3, 109.8, 119.3, 122.2, 122.5, 126.1, 126.6, 131.3, 134.0, 151.1.

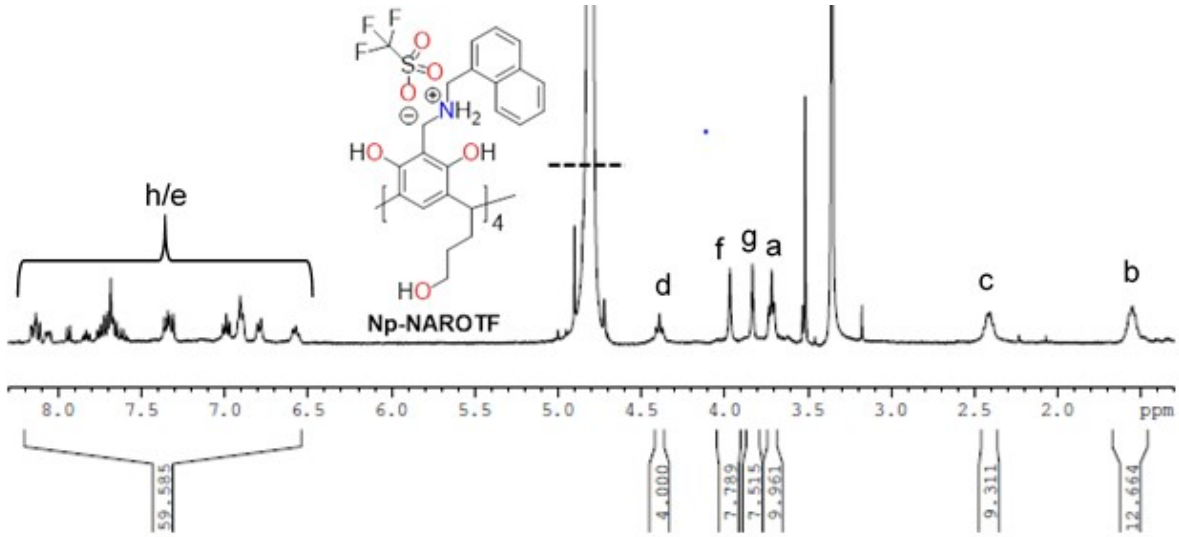

Figure S21. ^1H NMR of *N*-naphthyl ammonium resorcinarene triflate, NpNAROTf$_4$, in D_2O at 298 K.

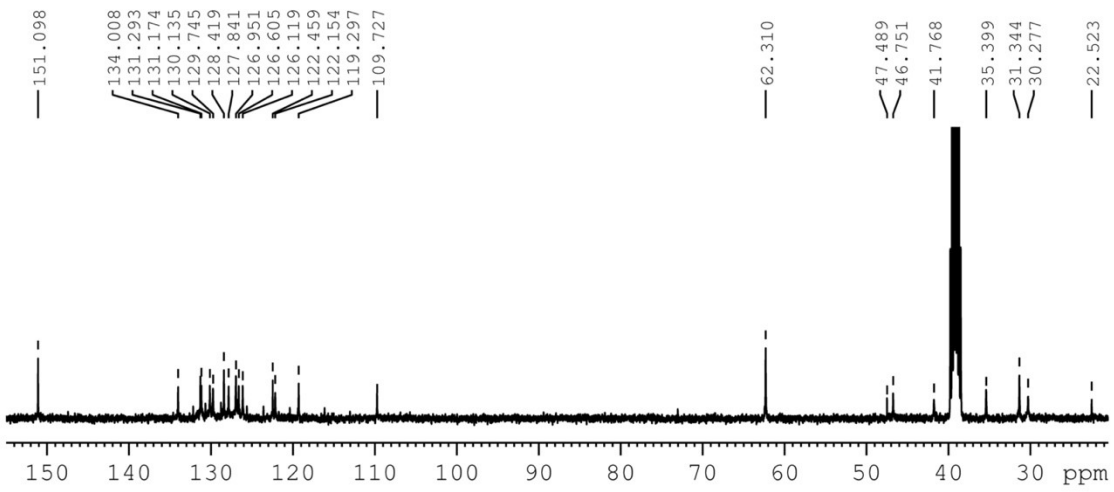

Figure S22. ^{13}C NMR of *N*-naphthyl ammonium resorcinarene triflate, NpNAROTf$_4$, in [D$_6$]DMSO at 298 K.

3. ISOTHERMAL TITRATION CALORIMETRY (ITC) EXPERIMENTS

VP-ITC instrument by MicroCal was used to determine the molar enthalpy (ΔH) of complexation. Subsequent fitting of the data to a 1:1 and 1:2 binding model using origin proprietary software provides association constants (K), change in enthalpy (ΔH) and change in entropy (ΔS). The ITC experiment was carried out by filling the sample cell with the receptor (0.25 mM) and filling the syringe with the phosphate titrants (5 mM), and titrating via computer-automated injector at 298 K. Blank titrations into plain solvent were also performed and subtracted from the corresponding titration to remove any effect from the heats of dilution from the titrant.

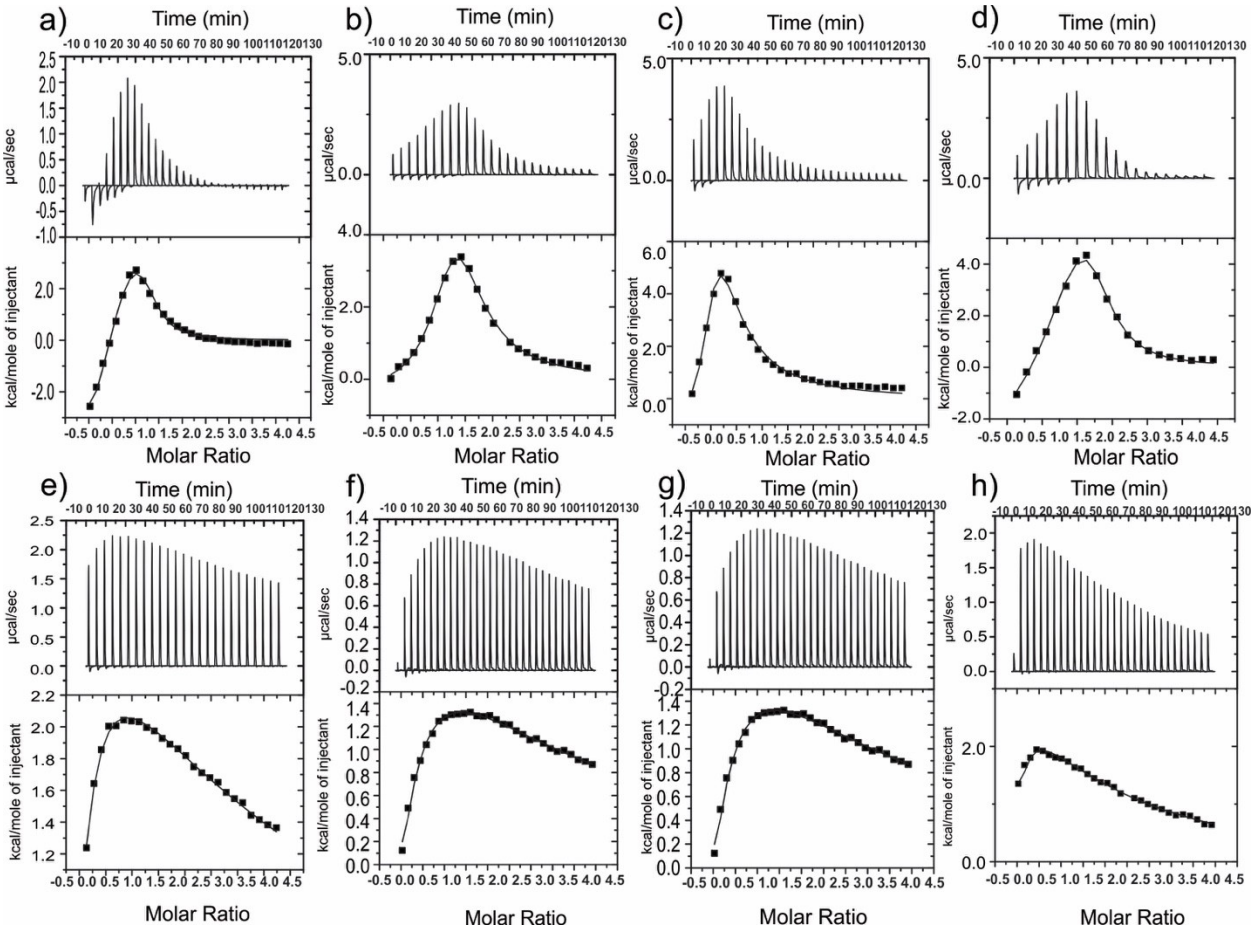

Figure S23. ITC traces of the titration of receptors with PPi at 298 K. The data was fitted to a two-sites binding model for (a) PPi@C3OHNAR$(Br)_4$, (b) PPi@CyNAR$(Br)_4$, (c) PPi@BnNAR$(OTf)_4$ and (d) PPi@NpNAR$(Br)_4$ in H_2O (90%) / DMSO (10%). (e) PPi@C3OHNAR$(Br)_4$ (f) PPi@CyNAR$(Br)_4$, (g) PPi@BnNAR$(Br)_4$ and (h) PPi@NpNAR$(Br)_4$ in Tris buffer pH 7.4 (90%) /DMSO (10%). The displaced anions are represented in parentheses.

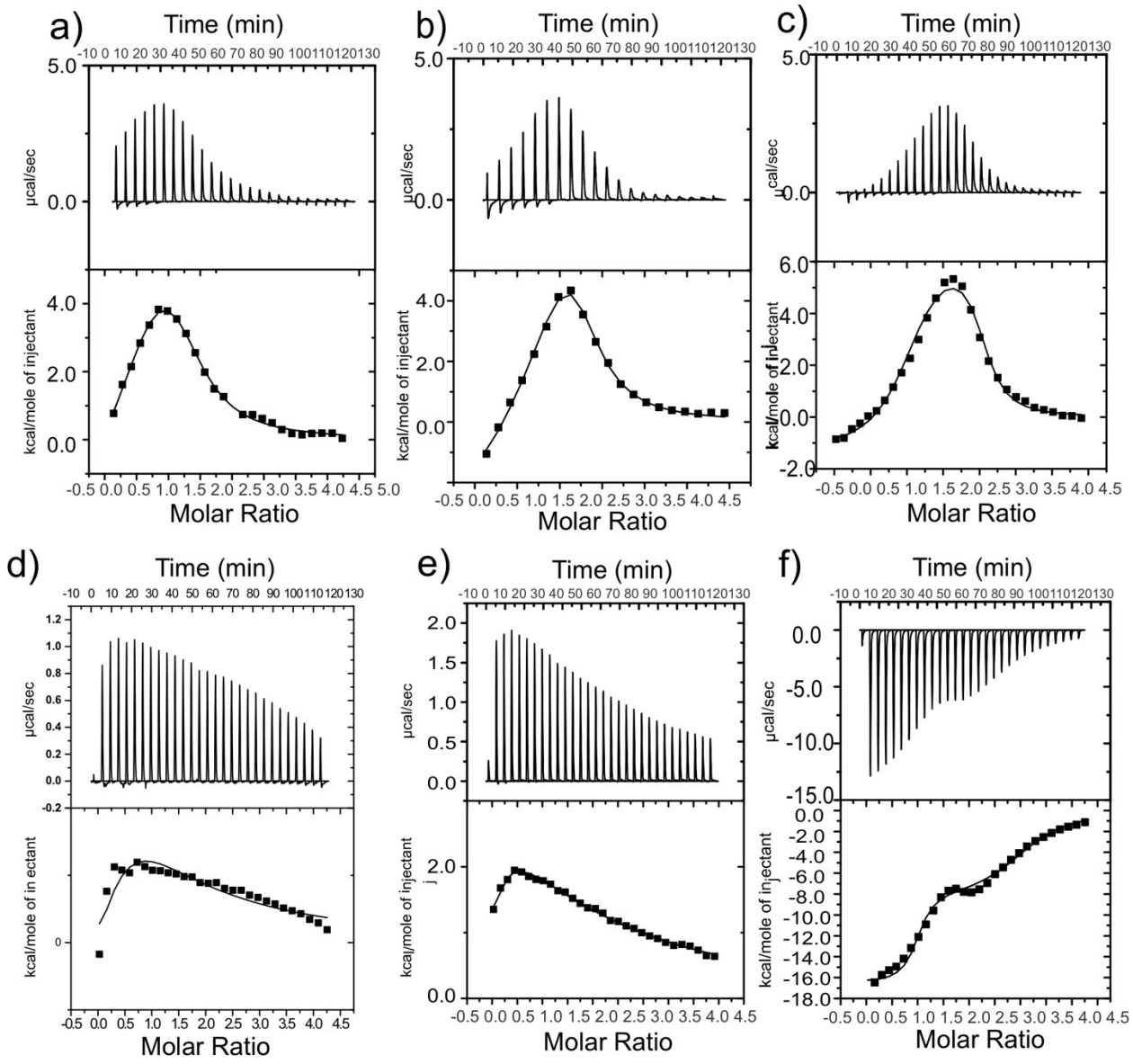

Figure S24. ITC traces of the titration of receptors with PPi at 298 K. The data was fitted to a two set of sites binding model for (a) PPi@NpNAR(Cl)$_4$, (b) PPi@NpNAR(Br)$_4$ and (c) PPi@NpNAR(OTf)$_4$ in 90% H_2O/10% DMSO. (d) PPi@NpNAR(Cl)$_4$, (e) PPi@NpNAR(Br)$_4$ and (f) PPi@NpNAR(OTf)$_4$ were fitted to two binding sites model in 90% Tris buffer pH 7.4/10% DMSO. The displaced anions are represented in parentheses.

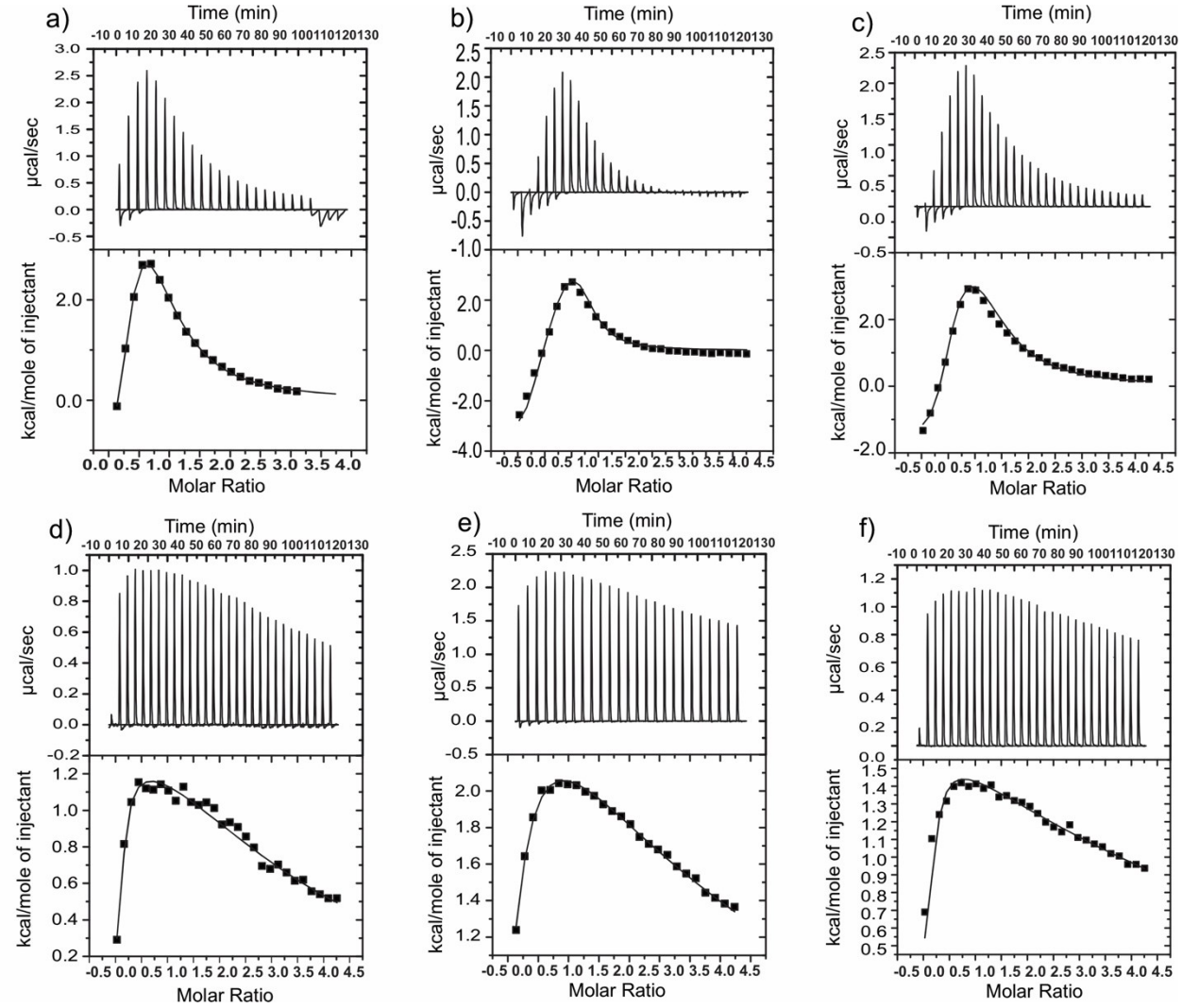

Figure S25. ITC traces of the titration of receptors with PPi at 298 K. The data was fitted to a two set of sites binding model for (a) PPi@C3OHNAR(Cl)$_4$, (b) PPi@C3OHNAR(Br)$_4$, (c) PPi@C3OHNAR(OTf)$_4$ in 90% H_2O/10% DMSO. (d) PPi@C3OHNAR(Cl)$_4$ (e) PPi@C3OHNAR(Br)$_4$ (f) PPi@C3OHNAR(OTf)$_4$ in 90% Tris buffer pH 7.4/10% DMSO. The displaced anions are represented in parentheses.

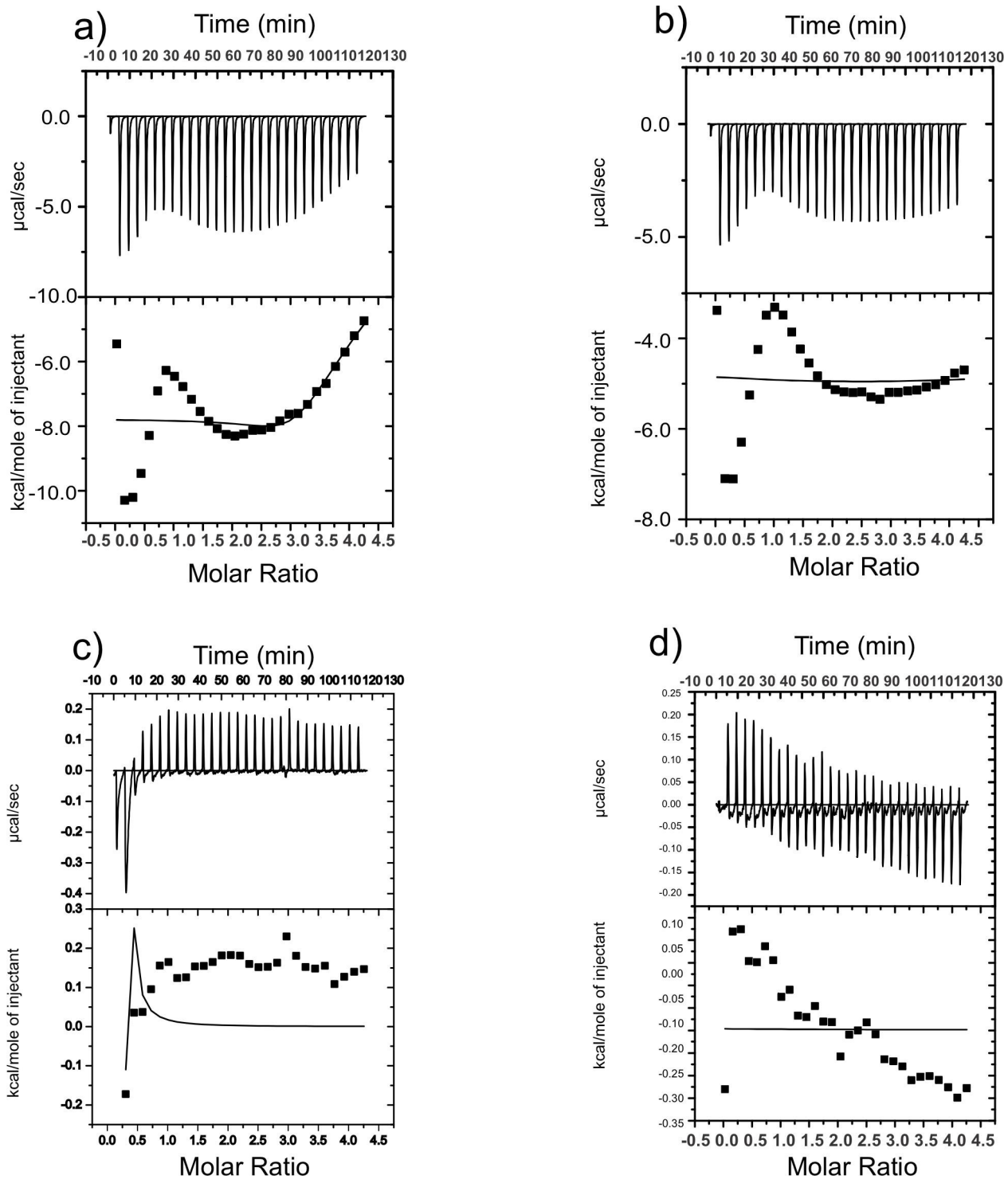

Figure S26. ITC traces of the titration of receptors with PO_4^- at 298 K. ITC data could not be fitted to any binding model for (a) PO_4^-@C3OHNAR$(Br)_4$, (b) PO_4^-@C3OHNAR$(OTf)_4$ in 90% H_2O/10% DMSO. (c) PO_4^-@C3OHNAR$(Br)_4$ (d) PO_4^-@C3OHNAR$(OTf)_4$ in 90% Tris buffer pH 7.4/10% DMSO. The displaced anions are represented in parentheses.

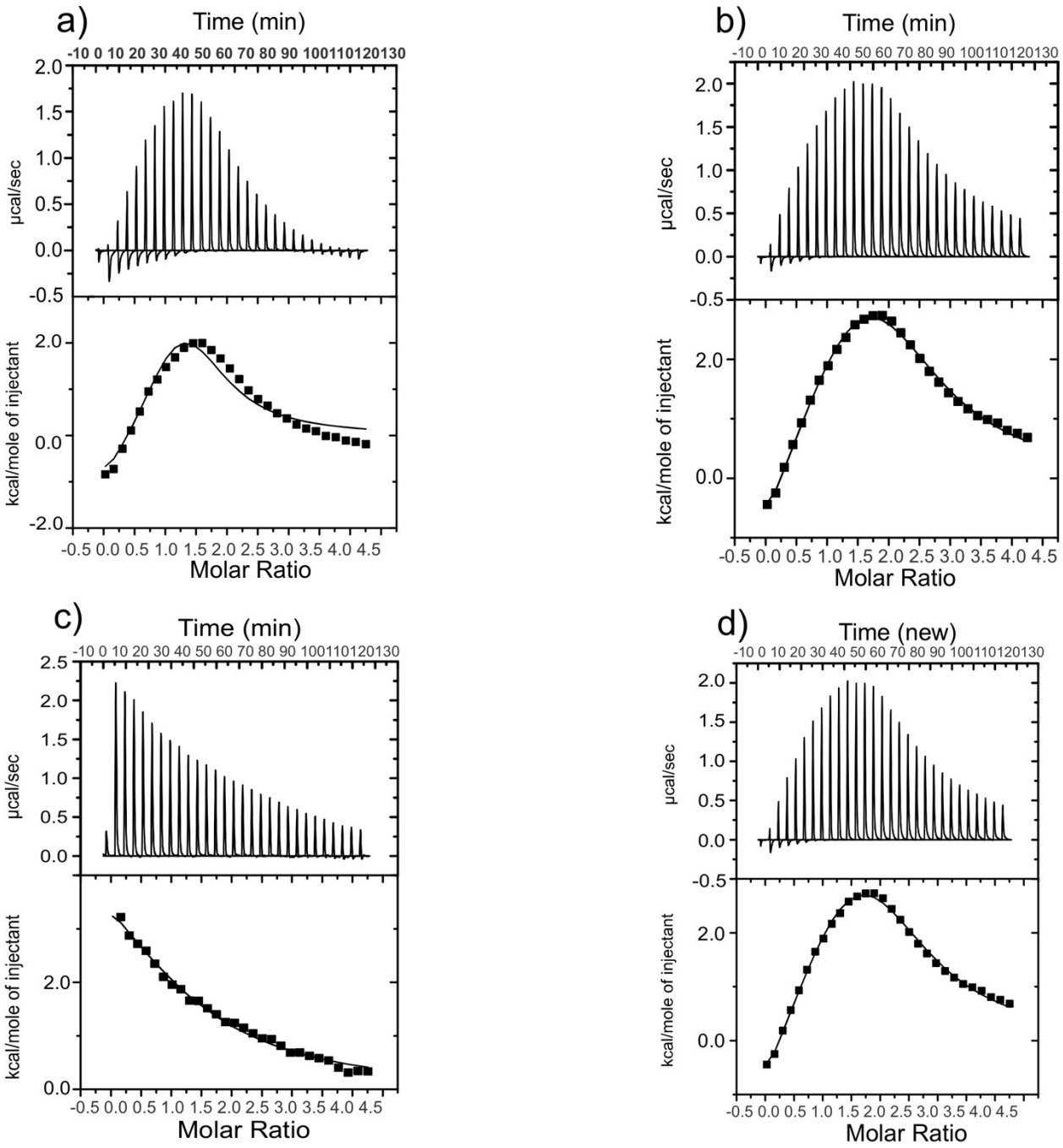

Figure S27. ITC traces of the titration of receptors with AMP at 298 K. ITC data was fitted to two set of sites binding model for (a) AMP@C3OHNAR(Br)$_4$ and (b) AMP@C3OHNAR(OTf)$_4$ in 90% H_2O/10% DMSO. (c) AMP@C3OHNAR(Br)$_4$ was fitted to one set of sites and (d) AMP@C3OHNAR(OTf)$_4$ to two set of sites in 90% Tris buffer pH 7.4/10% DMSO. The displaced anions are represented in parentheses.

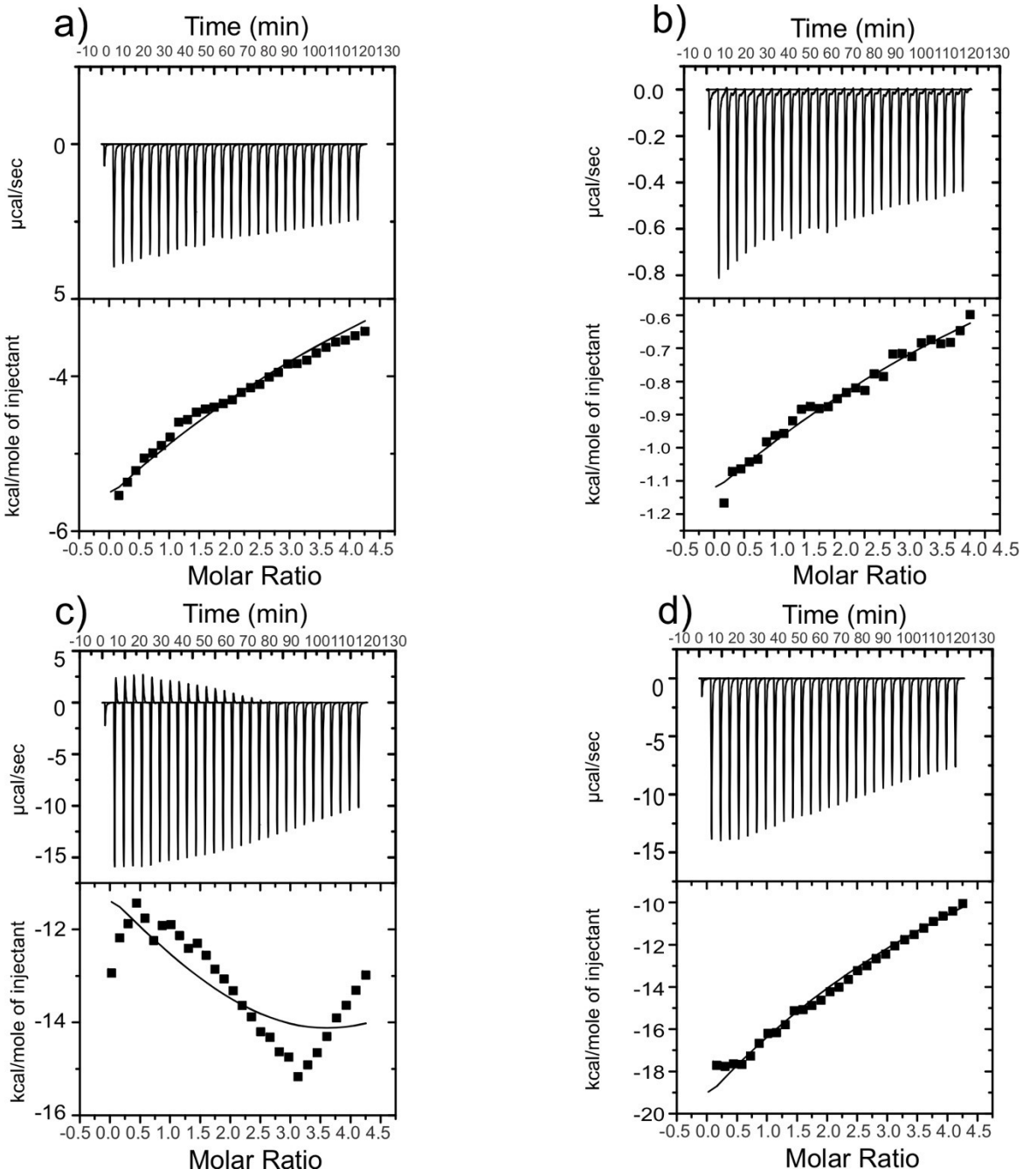

Figure S28. ITC traces of the titration of receptors with ADP at 298 K. ITC data was fitted to one set of sites binding model for (a) ADP@C3OHNAR$(Br)_4$ and (b) ADP@C3OHNAR$(OTf)_4$ in 90% H_2O/10% DMSO. (c) ADP@C3OHNAR$(Br)_4$ could not be fitted to any binding model and (d) ADP@C3OHNAR$(OTf)_4$ to one set of sites in 90% Tris buffer pH 7.4/10% DMSO. The displaced anions are represented in parentheses.

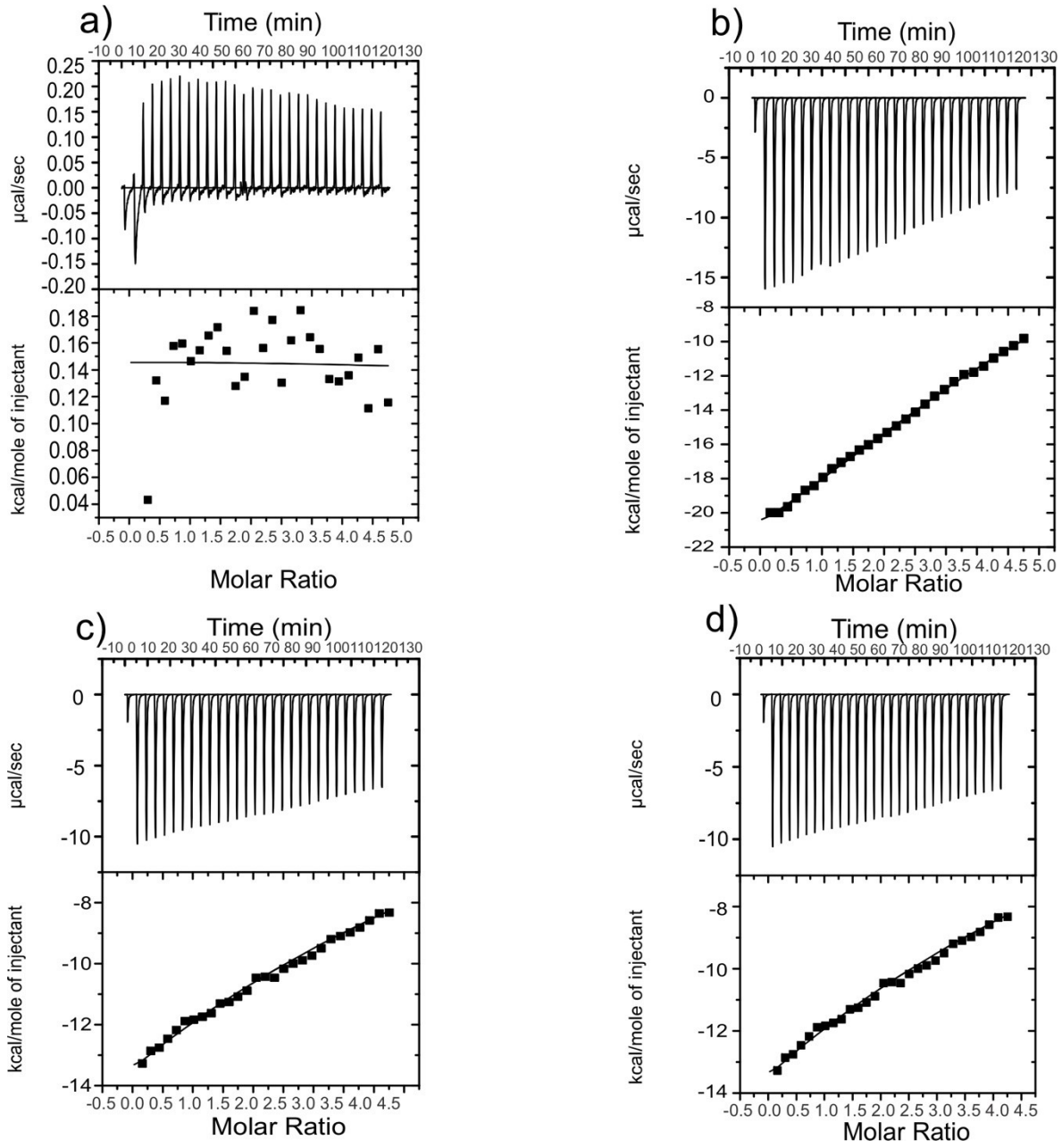

Figure S29. ITC traces of the titration of receptors with ATP at 298 K. ITC data could not be fitted to any binding model for (a) ATP@C3OHNAR$(Br)_4$. Data was fitted to one set of sites for (b) ATP@C3OHNAR$(OTf)_4$ in 90% H_2O/10% DMSO. (c) ATP@C3OHNAR$(Br)_4$ and (d) ATP@C3OHNAR$(OTf)_4$ were fitted to one set of sites in 90% Tris buffer pH 7.4/10% DMSO. The displaced anions are represented in parentheses.

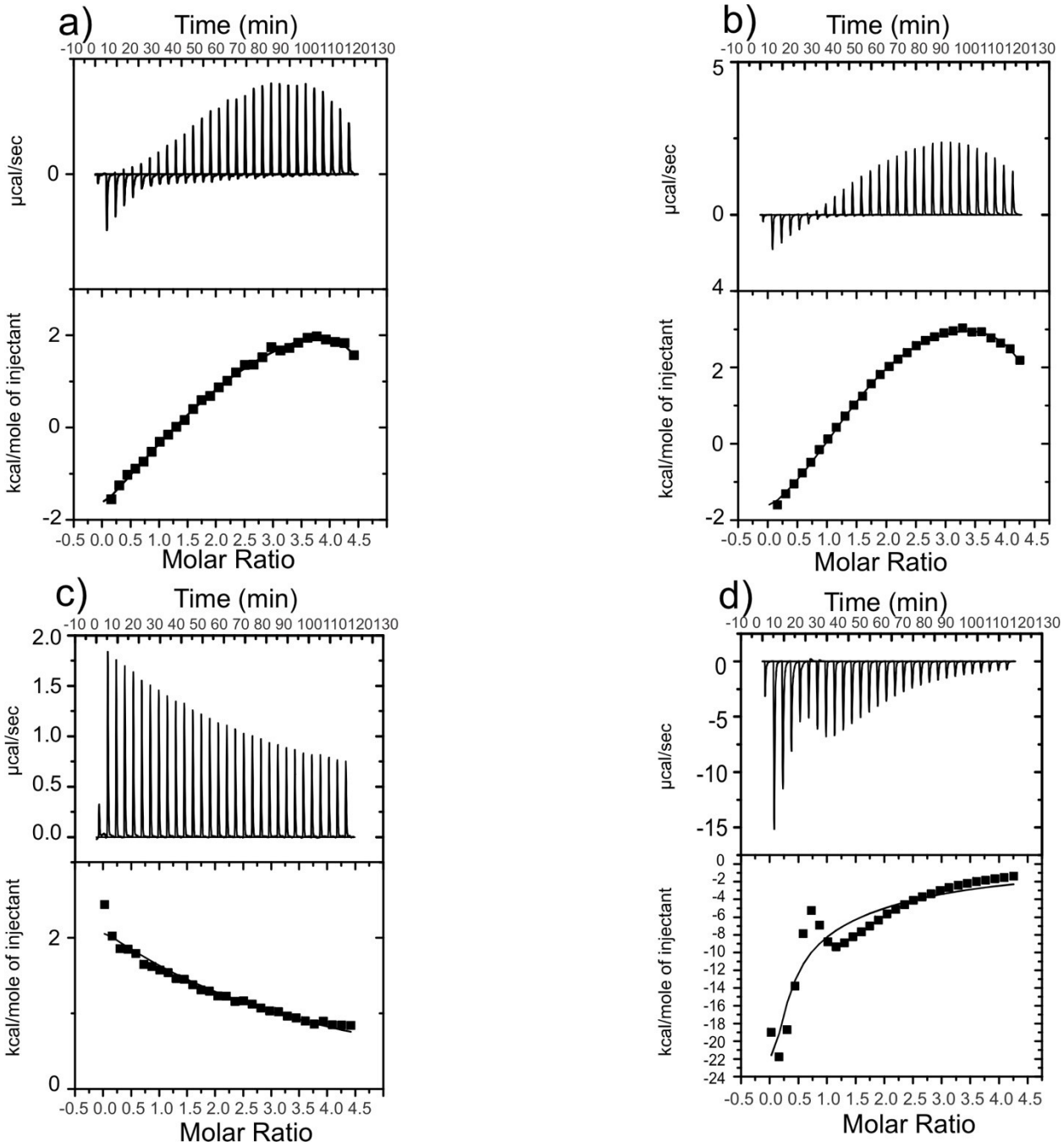

Figure S30. ITC traces of the titration of receptors with AMP at 298 K. ITC data was fitted to two set of sites binding model for (a) AMP@NpNAR(Br)$_4$ and (b) AMP@NpNAR(OTf)$_4$ in 90% H_2O/10% DMSO. (c) AMP@NpNAR(Br)$_4$ was fitted to one set of sites and (d) AMP@NpNAR(OTf)$_4$ could not be fitted to any binding model in 90% Tris buffer pH 7.4/10% DMSO. The displaced anions are represented in parentheses.

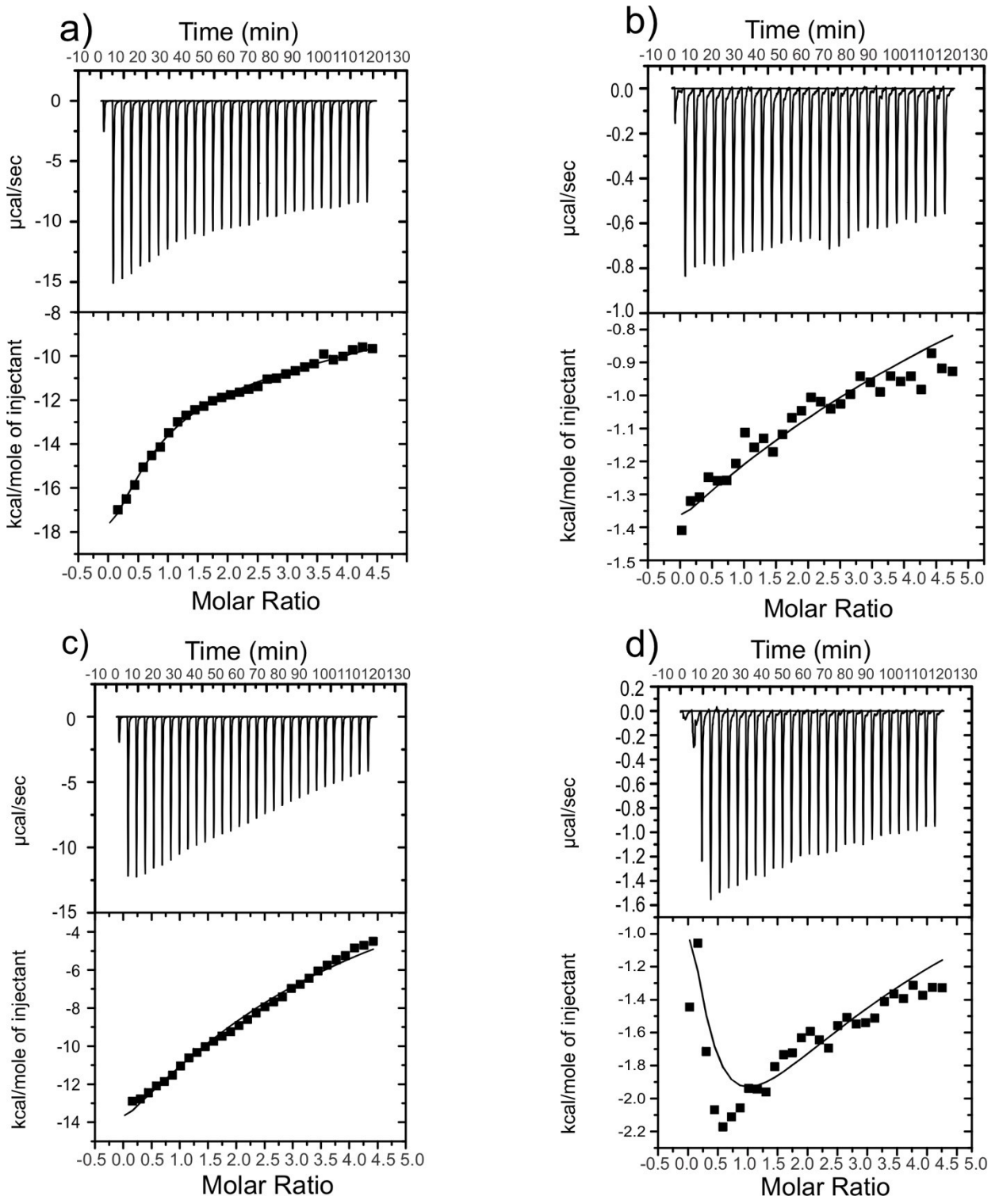

Figure S31. ITC traces of the titration of receptors with ADP at 298 K. ITC data was fitted to one set of sites binding model for (a) ADP@NpNAR(Br)$_4$ and (b) ADP@NpNAR(OTf)$_4$ in 90% H_2O/10% DMSO. (c) ADP@NpNAR(Br)$_4$ was fitted to one set of sites and (d) ADP@NpNAR(OTf)$_4$ could not be fitted to any binding model in 90% Tris buffer pH 7.4/10% DMSO. The displaced anions are represented in parentheses.

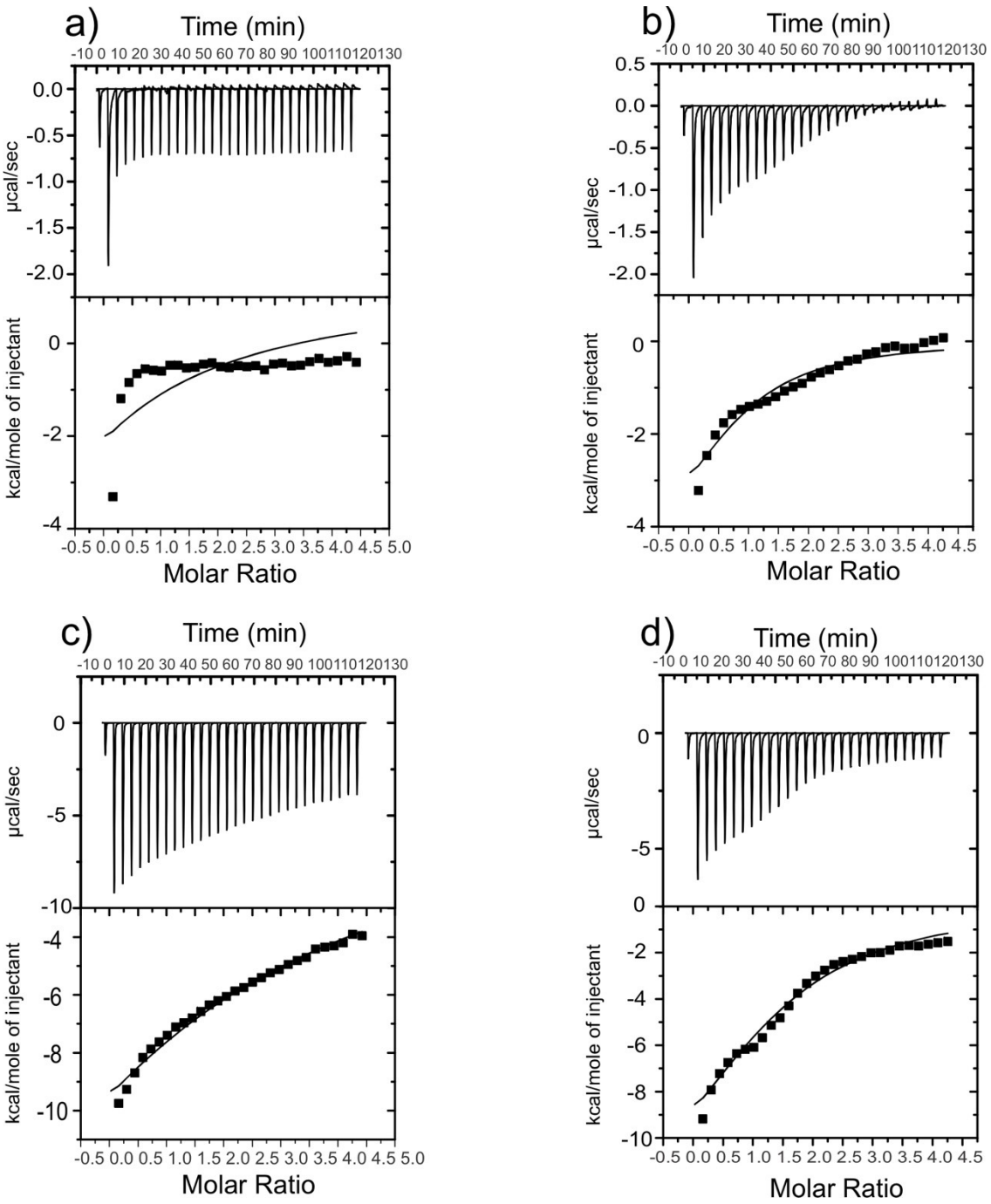

Figure S32. ITC traces of the titration of receptors with ATP at 298 K. ITC data could not be fitted for (a) ATP@NpNAR(Br)$_4$, data was fitted to one set of sites binding model for (b) ATP@NpNAR(OTf)$_4$ in 90% H_2O/10% DMSO. (c) ATP@NpNAR(Br)$_4$ and (d) ATP@NpNAR(OTf)$_4$ were fitted to one set of sites binding model in 90% Tris buffer pH 7.4/10% DMSO. The displaced anions are represented in parentheses.

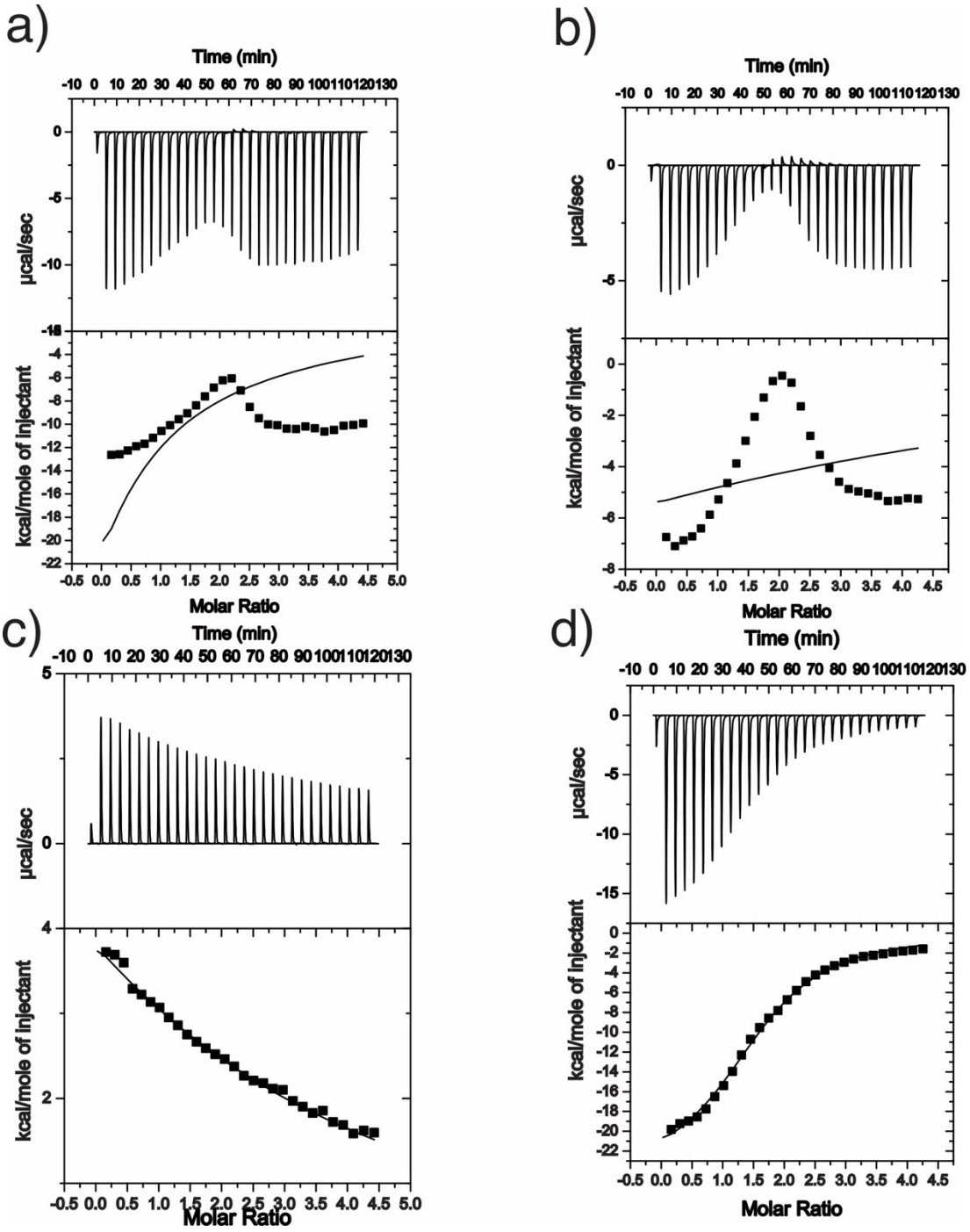

Figure S33. ITC traces of the titration of receptors with PO_4^- at 298 K. ITC data could not be fitted for (a) PO_4^-@NpNAR(Br)$_4$ and (b) PO_4^-@NpNAR(OTf)$_4$ in 90% H_2O/10% DMSO. (c) PO_4^-@NpNAR(Br)$_4$ and (d) PO_4^-@NpNAR(OTf)$_4$ were fitted to one set of sites binding model in 90% Tris buffer pH 7.4/10% DMSO. The displaced anions are represented in parentheses.

Table S1. Thermodynamic binding parameters of formed complexes between PPi@Cy-NAR(Br)$_4$ and PPi@Bn-NAR(Br)$_4$ in mixed buffer systems

Complex	K_1 ($\times 10^5$) M^{-1}	ΔH_1 kcal/mol	$T\Delta S_1$ kcal/mol	ΔG_1 kcal/mol	Complex	K_2 ($\times 10^5$) M^{-1}	ΔH_2 kcal/mol	$T\Delta S_2$ kcal/mol	ΔG_2 kcal/mol
PPi@CyNAR(Br)$_4$	1.3±0.1	-6.5±1.4	-0.9	-5.6	PPi@CyNAR(Br)$_4$	0.9±0.2	13±1.1	17	-4.0
PPi@BnNAR(Br)$_4$	3.6±0.6	-1.0±0.4	5.2	-6.2	PPi@BnNAR(Br)$_4$	1.4±0.1	9.8±0.4	14	-4.2

Table S2. Thermodynamic binding parameters of formed complexes between PPi@C3OH-NAR(X) in mixed water and buffer systems

Complex	K_1 ($\times 10^5$) M^{-1}	ΔH_1 kcal/mol	$T\Delta S_1$ kcal/mol	ΔG_1 kcal/mol	Complex	K_1 ($\times 10^4$) M^{-1}	ΔH_1 kcal/mol	$T\Delta S_1$ kcal/mol	ΔG_1 kcal/mol
PPi@C3OH-NAR(Cl)$_4$	3.6±0.3	-1.7±0.2	5.9	-7.6	PPi@C3OH-NAR(Cl)$_4$	2.0±0.2	-4.5±0.6	1.4	-5.9
					PPi@C3OH-NAR(Br)$_4$	6.1±0.8	3.6±0.2	10	-6.5
PPi@C3OH-NAR(OTf)$_4$	6.2±0.8	5.7±0.3	14	-7.9	PPi@C3OH-NAR(OTf)$_4$	7.4±0.8	-1.5±0.4	5.1	-6.6
Complex	K_2 ($\times 10^5$) M^{-1}	ΔH_2 kcal/mol	$T\Delta S_2$ kcal/mol	ΔG_2 kcal/mol	**Complex**	K_2 ($\times 10^3$) M^{-1}	ΔH_2 kcal/mol	$T\Delta S_2$ kcal/mol	ΔG_2 kcal/mol
PPi@C3OH-NAR(Cl)$_4$	0.6±0.1	6.7±0.1	13	-6.1	PPi@C3OH-NAR(Cl)$_4$	0.8±0.01	1.8±0.1	22	-21
					PPi@C3OH-NAR(Br)$_4$	2.2±0.8	2.1±0.1	7.2	-5.1
PPi@C3OH-NAR(OTf)$_4$	4.6±2.1	-4.1±0.2	2.2	-6.2	PPi@C3OH-NAR(OTf)$_4$	0.7±0.2	4.5±1.1	8.4	-3.9
90% H20/10% DMSO					90% BUFFER/10% DMSO				

Table S3. Thermodynamic binding parameters of formed complexes between PPi@Np-NAR(X) in mixed water and buffer systems

Complex	K_1 ($\times 10^5$) M^{-1}	ΔH_1 kcal/mol	$T\Delta S_1$ kcal/mol	ΔG_1 kcal/mol	Complex	K_1 ($\times 10^5$) M^{-1}	ΔH_1 kcal/mol	$T\Delta S_1$ kcal/mol	ΔG_1 kcal/mol
					PPi@Np-NAR(Cl)$_4$	2.0±0.2	-4.5±0.6	1.3	-5.8
					PPi@Np-NAR(Br)$_4$	6.3±1.6	0.4±0.3	6.7	-6.2
					PPi@Np-NAR(OTf)$_4$	7.4±0.8	-1.5±0.4	4.8	-6.3
Complex	K_2 ($\times 10^5$) M^{-1}	ΔH_2 kcal/mol	$T\Delta S_2$ kcal/mol	ΔG_2 kcal/mol	**Complex**	K_2 ($\times 10^3$) M^{-1}	ΔH_2 kcal/mol	$T\Delta S_2$ kcal/mol	ΔG_2 kcal/mol
					PPi@Np-NAR(Cl)$_4$	0.8±0.1	0.8±0.1	22	-22
					PPi@Np-NAR(Br)$_4$	5.2±0.8	2.10±0.1	7.2	-5.1
					PPi@Np-NAR(OTf)$_4$	0.8±0.3	4.5±1.1	8.4	-3.9
90% H20/10% DMSO					90% BUFFER/10% DMSO				

Table S4. Thermodynamic binding parameters of formed complexes between PO_4@C3OH-NAR(X) in mixed water and buffer systems

Complex	K_1 ($\times 10^5$) M^{-1}	ΔH_1 kcal/mol	$T\Delta S_1$ kcal/mol	ΔG_1 kcal/mol	Complex	K_1 ($\times 10^5$) M^{-1}	ΔH_1 kcal/mol	$T\Delta S_1$ kcal/mol	ΔG_1 kcal/mol
PO_4@C3OH-NAR(Br)$_4$	Does not fit				PO_4@C3OH-NAR(Br)$_4$	Does not fit			
PO_4@COH-NAR(OTf)$_4$	Does not fit				PO_4@COH-NAR(OTf)$_4$	Does not fit			
Complex	K_2 ($\times 10^5$) M^{-1}	ΔH_2 kcal/mol	$T\Delta S_2$ kcal/mol	ΔG_2 kcal/mol	**Complex**	K_2 ($\times 10^5$) M^{-1}	ΔH_2 kcal/mol	$T\Delta S_2$ kcal/mol	ΔG_2 kcal/mol
PO_4@C3OH-NAR(Br)$_4$	Does not fit				PO_4@C3OH-NAR(Br)$_4$	Does not fit			
PO_4@COH-NAR(OTf)$_4$	Does not fit				PO_4@COH-NAR(OTf)$_4$	Does not fit			
90% H20/10% DMSO					90% BUFFER/10% DMSO				

Table S5. Thermodynamic binding parameters of formed complexes between AMP@C3OH-NAR(X) in mixed water and buffer systems

Complex	K_1 ($\times 10^4$) M^{-1}	ΔH_1 kcal/mol	$T\Delta S_1$ kcal/mol	ΔG_1 kcal/mol	Complex	K_1 ($\times 10^4$) M^{-1}	ΔH_1 kcal/mol	$T\Delta S_1$ kcal/mol	ΔG_1 kcal/mol
AMP@C3OH-NAR(Br)$_4$	3.5±0.7	9.6±1.5	16	-6.2	AMP@C3OH-NAR(Br)$_4$	0.7±0.1	6.2±0.7	11	-5.2
AMP@C3OH-NAR(OTf)$_4$	5.7±0.4	-5.2±0.3	1.3	-6.5	AMP@C3OH-NAR(OTf)$_4$	5.5±0.5	-5.9±1.2	0.6	-6.5
Complex	K_2 ($\times 10^5$) M^{-1}	ΔH_2 kcal/mol	$T\Delta S_2$ kcal/mol	ΔG_2 kcal/mol	**Complex**	K_2 ($\times 10^4$) M^{-1}	ΔH_2 kcal/mol	$T\Delta S_2$ kcal/mol	ΔG_2 kcal/mol
AMP@C3OH-NAR(Br)$_4$	1.4±4.0	-2.5±1.0	4.5	-7	AMP@C3OH-NAR(Br)$_4$	-	-	-	-
AMP@COH-NAR(OTf)$_4$	0.2±0.03	1.4±0.2	20	-18	AMP@C3OH-NAR(OTf)$_4$	2.2±0.1	15±1.4	21	-5.9
90% H20/10% DMSO					90% BUFFER/10% DMSO				

Table S6. Thermodynamic binding parameters of formed complexes between ADP@C3OH-NAR(X) in mixed water and buffer systems

Complex	K_1 ($\times 10^2$) M^{-1}	ΔH_1 kcal/mol	$T\Delta S_1$ kcal/mol	ΔG_1 kcal/mol	Complex	K_1 ($\times 10^2$) M^{-1}	ΔH_1 kcal/mol	$T\Delta S_1$ kcal/mol	ΔG_1 kcal/mol
ADP@C3OH-NAR(Br)$_4$	1.7±0.2	-105±13	-102	-3.1	ADP@C3OH-NAR(Br)$_4$	Does not fit	-	-	-
ADP@C3OH-NAR(OTf)$_4$	7±0.2	-3.2±0.5	0.6	-3.9	AMP@COH-NAR(OTf)$_4$	3.0±0.2	-434±26	-429	-4.9
Complex	K_2 ($\times 10^5$) M^{-1}	ΔH_2 kcal/mol	$T\Delta S_2$ kcal/mol	ΔG_2 kcal/mol	**Complex**	K_2 ($\times 10^4$) M^{-1}	ΔH_2 kcal/mol	$T\Delta S_2$ kcal/mol	ΔG_2 kcal/mol
ADP@C3OH-NAR(Br)$_4$	-	-	-	-	ADP@C3OH-NAR(Br)$_4$	-	-	-	-
ADP@C3OH-NAR(OTf)$_4$	-	-	-	-	ADP@C3OH-NAR(OTf)$_4$	-	-	-	-
90% H20/10% DMSO					90% BUFFER/10% DMSO				

Table S7. Thermodynamic binding parameters of formed complexes between ATP@C3OH-NAR(X) in mixed water and buffer systems

Complex	K_1 ($\times 10^3$) M^{-1}	ΔH_1 kcal/mol	$T\Delta S_1$ kcal/mol	ΔG_1 kcal/mol	Complex	K_1 ($\times 10^1$) M^{-1}	ΔH_1 kcal/mol	$T\Delta S_1$ kcal/mol	ΔG_1 kcal/mol
ATP@C3OH-NAR(Br)$_4$	Does not fit	-	-	-	ATP@C3OH-NAR(Br)$_4$	9.4±1	-1151±115	-1147	-3.7
ATP@C3OH-NAR(OTf)$_4$	3.4±0.2	-30±0.7	-25	-4.8	ATP@C3OH-NAR(OTf)$_4$	10.7±1.3	-898±100	-894	-64
Complex	K_2 ($\times 10^5$) M^{-1}	ΔH_2 kcal/mol	$T\Delta S_2$ kcal/mol	ΔG_2 kcal/mol	**Complex**	K_2 ($\times 10^4$) sM^{-1}	ΔH_2 kcal/mol	$T\Delta S_2$ kcal/mol	ΔG_2 kcal/mol
ATP@C3OH-NAR(Br)$_4$	-	-	-	-	ATP@C3OH-NAR(Br)$_4$	-	-	-	-
ATP@C3OH-NAR(OTf)$_4$	-	-	-	-	ATP@C3OH-NAR(OTf)$_4$	-	-	-	-
	90% H20/10% DMSO					90% BUFFER/10% DMSO			

Table S8. Thermodynamic binding parameters of formed complexes between PO_4@Np-NAR(X) in mixed water and buffer systems

Complex	K_1 ($\times 10^5$) M^{-1}	ΔH_1 kcal/mol	$T\Delta S_1$ kcal/mol	ΔG_1 kcal/mol	Complex	K_1 ($\times 10^4$) M^{-1}	ΔH_1 kcal/mol	$T\Delta S_1$ kcal/mol	ΔG_1 kcal/mol
PO4@Np-NAR(Br)$_4$	Does not fit				PO4@Np-NAR(Br)$_4$	0.1±0.004	13±5.1	17	-4.3
PO4@Np-NAR(OTf)$_4$	Does not fit				PO4@Np-NAR(OTf)$_4$	2.7±0.2	-25±0.5	-19	-6.0
Complex	K_2 ($\times 10^5$) M^{-1}	ΔH_2 kcal/mol	$T\Delta S_2$ kcal/mol	ΔG_2 kcal/mol	**Complex**	K_2 ($\times 10^5$) M^{-1}	ΔH_2 kcal/mol	$T\Delta S_2$ kcal/mol	ΔG_2 kcal/mol
PO4@Np-NAR(Br)$_4$	Does not fit				PO4@Np-NAR(Br)$_4$	-	-	-	-
PO4@Np-NAR(OTf)$_4$	Does not fit				PO4@Np-NAR(OTf)$_4$	-	-	-	-
	90% H20/10% DMSO					90% BUFFER/10% DMSO			

Table S9. Thermodynamic binding parameters of formed complexes between AMP@Np-NAR(X) in mixed water and buffer systems

Complex	K_1 ($\times 10^4$) M^{-1}	ΔH_1 kcal/mol	$T\Delta S_1$ kcal/mol	ΔG_1 kcal/mol	Complex	K_1 ($\times 10^3$) M^{-1}	ΔH_1 kcal/mol	$T\Delta S_1$ kcal/mol	ΔG_1 kcal/mol
AMP@Np-NAR(Br)$_4$	1.2±0.6	-5.9±0.9	2.4	-8.3	AMP@Np-NAR(Br)$_4$	1.4±0.2	7.3±0.6	12	-4.3
AMP@Np-NAR(OTf)$_4$	2±0.5	-3.3±0.2	5.3	-8.6	AMP@Np-NAR(OTf)$_4$	Does not fit	-	-	-
Complex	K_2 ($\times 10^3$) M^{-1}	ΔH_2 kcal/mol	$T\Delta S_2$ kcal/mol	ΔG_2 kcal/mol	**Complex**	K_2 ($\times 10^4$) M^{-1}	ΔH_2 kcal/mol	$T\Delta S_2$ kcal/mol	ΔG_2 kcal/mol
AMP@Np-NAR(Br)$_4$	3.8±1.34	3.7±0.4	11	-7.6	AMP@Np-NAR(Br)$_4$	-	-	-	-
AMP@Np-NAR(OTf)$_4$	2.6±0.4	4.0±0.1	11	-7.4	AMP@Np-NAR(OTf)$_4$	-	-	-	-
	90% H20/10% DMSO					90% BUFFER/10% DMSO			

Table S10. Thermodynamic binding parameters of formed complexes between ADP@Np-NAR(X) in mixed water and buffer systems

Complex	K_1 ($\times 10^2$) M^{-1}	ΔH_1 kcal/mol	$T\Delta S_1$ kcal/mol	ΔG_1 kcal/mol	Complex	K_1 ($\times 10^4$) M^{-1}	ΔH_1 kcal/mol	$T\Delta S_1$ kcal/mol	ΔG_1 kcal/mol
ADP@Np-NAR(Br)$_4$	5.1±0.3	-19±4.4	-15	-3.7	ADP@Np-NAR(Br)$_4$	0.2±0.1	-31±5.7	-24	-6.3
ADP@Np-NAR(OTf)$_4$	1.4±0.4	-82±2.1	-79	-2.8	ADP@Np-NAR(OTf)$_4$	2.4±2	1.2±2.7	7.2	-6
Complex	K_2 ($\times 10^4$) M^{-1}	ΔH_2 kcal/mol	$T\Delta S_2$ kcal/mol	ΔG_2 kcal/mol	**Complex**	K_2 ($\times 10^2$) M^{-1}	ΔH_2 kcal/mol	$T\Delta S_2$ kcal/mol	ΔG_2 kcal/mol
ADP@Np-NAR(Br)$_4$	4.2±0.7	-23±3	-17	-6.3	ADP@Np-NAR(Br)$_4$	-	-	-	-
ADP@Np-NAR(OTf)$_4$	-	-	-	-	ADP@Np-NAR(OTf)$_4$	8.2±4.2	-18±5.1	-14	-4
90% H20/10% DMSO					90% BUFFER/10% DMSO				

Table S11. Thermodynamic binding parameters of formed complexes between ATP@Np-NAR(X) in mixed water and buffer systems

Complex	K_1 ($\times 10^2$) M^{-1}	ΔH_1 kcal/mol	$T\Delta S_1$ kcal/mol	ΔG_1 kcal/mol	Complex	K_1 ($\times 10^3$) M^{-1}	ΔH_1 kcal/mol	$T\Delta S_1$ kcal/mol	ΔG_1 kcal/mol
ATP@Np-NAR(Br)$_4$	Does not fit	-	-	-	ATP@Np-NAR(Br)$_4$	1.1±0.1	-34±1.5	-30	-4.1
ATP@Np-NAR(OTf)$_4$	Does not fit	-	-	-	ATP@Np-NAR(OTf)$_4$	Does not fit	-	-	-
Complex	K_2 ($\times 10^4$) M^{-1}	ΔH_2 kcal/mol	$T\Delta S_2$ kcal/mol	ΔG_2 kcal/mol	**Complex**	K_2 ($\times 10^2$) M^{-1}	ΔH_2 kcal/mol	$T\Delta S_2$ kcal/mol	ΔG_2 kcal/mol
ATP@Np-NAR(Br)$_4$	-	-	-	-	ATP@Np-NAR(Br)$_4$	-	-	-	-
ATP@Np-NAR(OTf)$_4$	-	-	-	-	ATP@Np-NAR(OTf)$_4$	-	-	-	-
90% H20/10% DMSO					90% BUFFER/10% DMSO				

4. NMR SPECTROSCOPY

For the pure samples' preparation, 2 mM stock solutions of either the receptors or the phosphates were prepared in 90 % D_2O, 10 % [D_6]DMSO. For pure receptors, 250 µl of the stock solution was pipetted into NMR tube and diluted with 250µl of 90 % D_2O, 10 % [D_6]DMSO pure solvent to give 1 mM sample concentration.

For 1:1 host-guest (receptor-phosphate) mixtures, 250 µl of the host and 250 µl of the guests were pipetted into an NMR tube to give a 1 mM concentration ratio of hosts and guests. The ^{1}H NMR were collected were calibrated using D_2O signal as internal standard. For ^{31}P NMR, concentrated H_3PO_4 in a 2 mm NMR tube was inserted into the sample as an external calibrant, calibrated at 0 ppm.

For NMR titration experiment, stock solutions of 10mM C3OH-NAR(Br)$_4$, C3OH-NAR(Otf)$_4$ and 100mM of PPi were prepared in 100% D_2O. 100ul of the PPi solution was titrated into an NMR tube containing 500ul of stock receptor solution to give equivalence of 0.20, 0.38, 0.57, 0.74, 0.91, 1.07, 1.23, 1.38, 1.53, 1.74, 1.94, 2.13 and 2.96.

For Job's plot measurement, 10 mM concentration of the host and guest were prepared.[5] 12 NMR samples were prepared with host-guest ratio of 0.00:0.50, 0.05:0.45, 0.10:0.40, 0.15:0.35, 0.20:0.30, 0.25:0.25, 0.30:0.20, 0.35:0.15, 0.40:0.10, 0.45:0.05, 0.50:0.00. The y-axis is the chemical shift change of the host. The X-axis is the mole fraction.

a) Job Plot Spectra

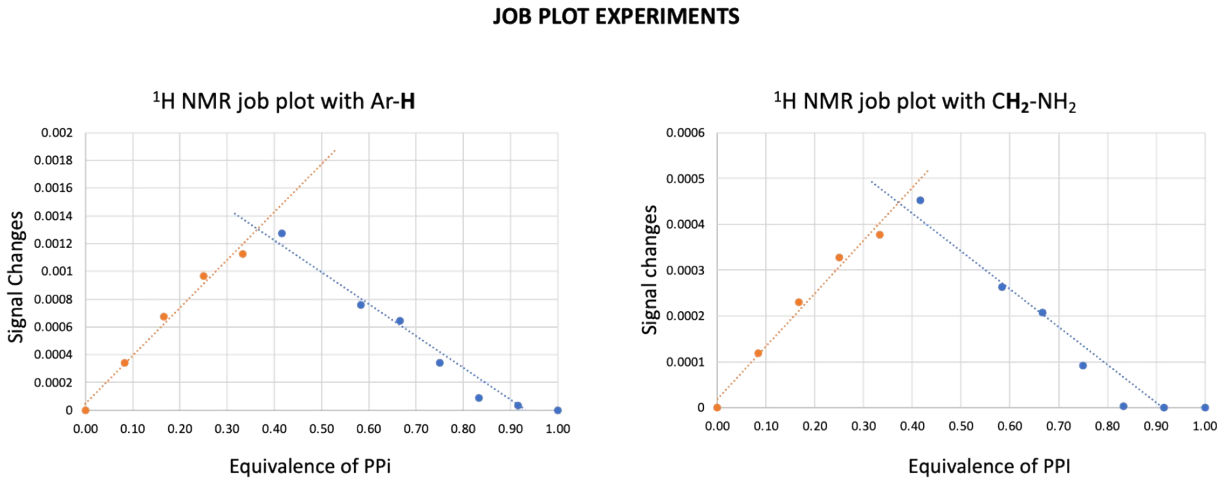

Figure S34. Job Plot of the binding pocket's aromatic (left) and methylene (right) H-NMR signal changes per equivalence of PPi added.

b) ^{1}H-NMR Spectra

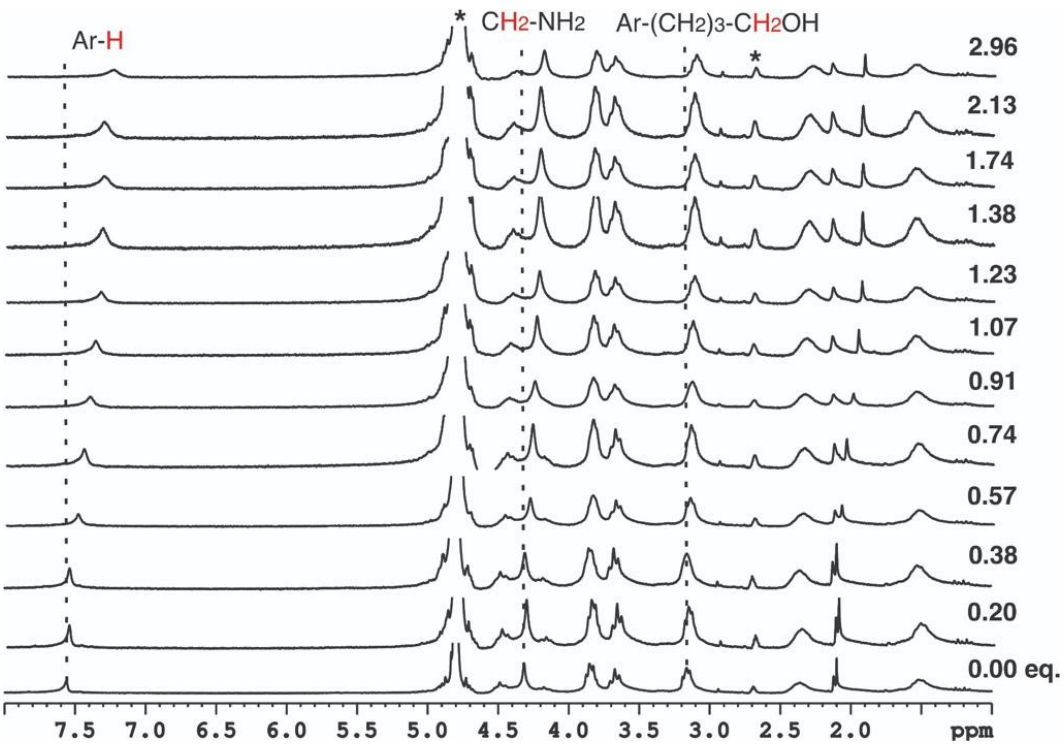

Figure S35. ^{1}H NMR titration spectra (D_2O, 298 K) of C_3OH-NAR$(Br)_4$ showing signal changes per equivalence of pyrophosphate added.

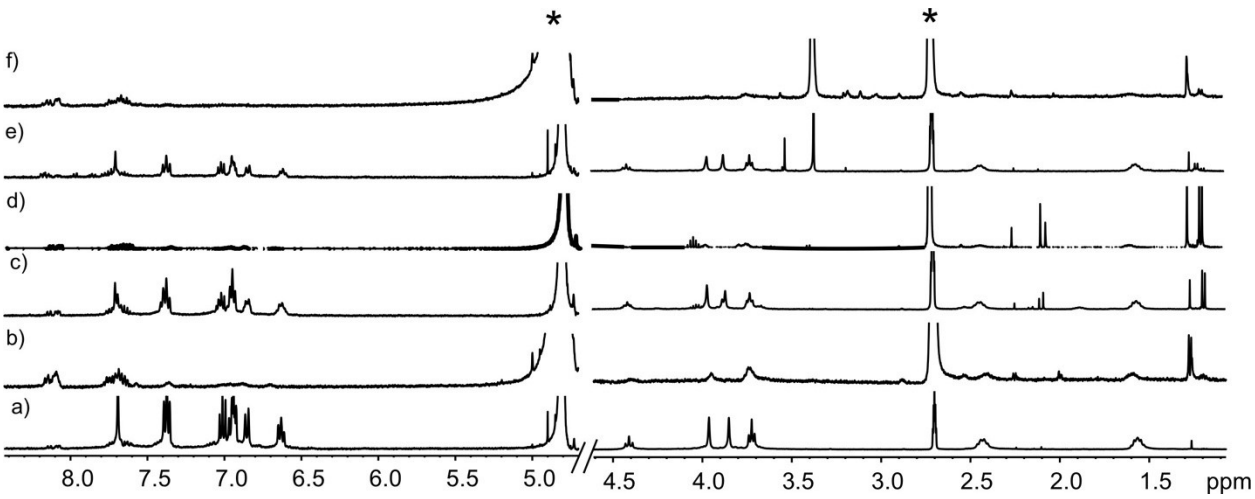

Figure S36. ^{1}H NMR spectra (D_2O/[D_6]DMSO 9/1 v/v, 298 K) of the pure host: (a) NpNARCl_4, (c) NpNARBr_4, (e) NpNAROTf_4, and equimolar mixtures of (b) PPi@NpNAR$(Cl)_4$, (b) PPi@NpNAR$(Br)_4$, (b) PPi@NpNAR$(OTf)_4$. The displaced anions are represented in parentheses. Star represents the residual D_2O solvent. The dash lines give an indication of the signal changes in ppm.

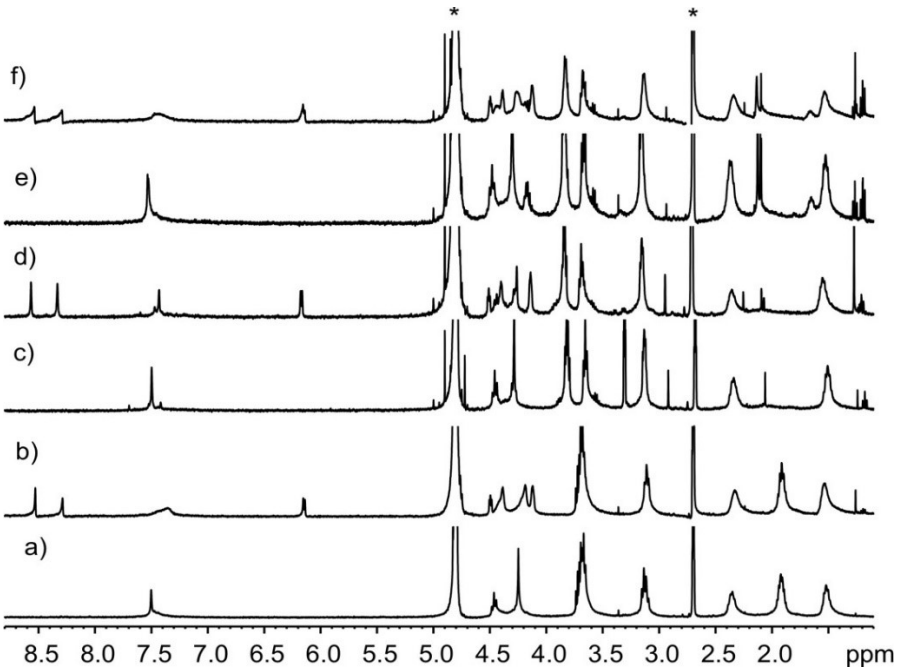

Figure S37. ^{1}H NMR spectra (D_2O/[D_6]DMSO 9/1 v/v, 298 K) of the pure host: (a) C3OHNARCl_4, (c) C3OHNARBr_4, (e) C3OHNAROTf_4, and equimolar mixtures of (b) AMP@C3OHNAR$(Cl)_4$, (b) AMP@C3OHNAR$(Br)_4$, (b) AMP@C3OHNAR$(OTf)_4$. The displaced anions are represented in parentheses. Star represents the residual D_2O solvent. The dash lines give an indication of the signal changes in ppm.

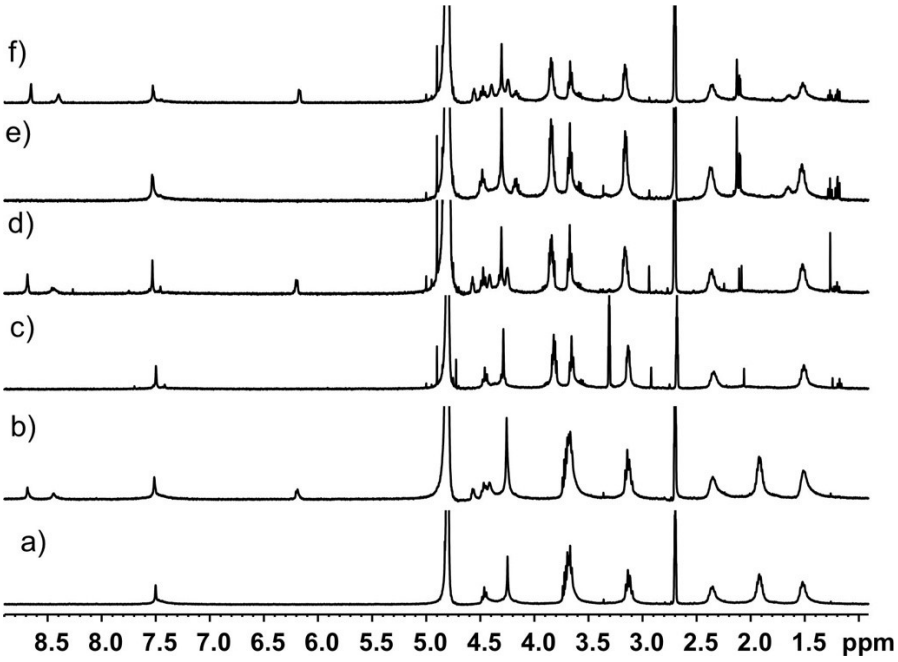

Figure S38. ^{1}H NMR spectra (D_2O/[D_6]DMSO 9/1 v/v, 298 K) of the pure host: (a) C3OHNARCl_4, (c) C3OHNARBr_4, (e) C3OHNAROTf_4, and equimolar mixtures of (b) ADP@C3OHNAR$(Cl)_4$, (b) ADP@C3OHNAR$(Br)_4$, (b) ADP@C3OHNAR$(OTf)_4$. The displaced anions are represented in parentheses. Star represents the residual D_2O solvent. The dash lines give an indication of the signal changes in ppm.

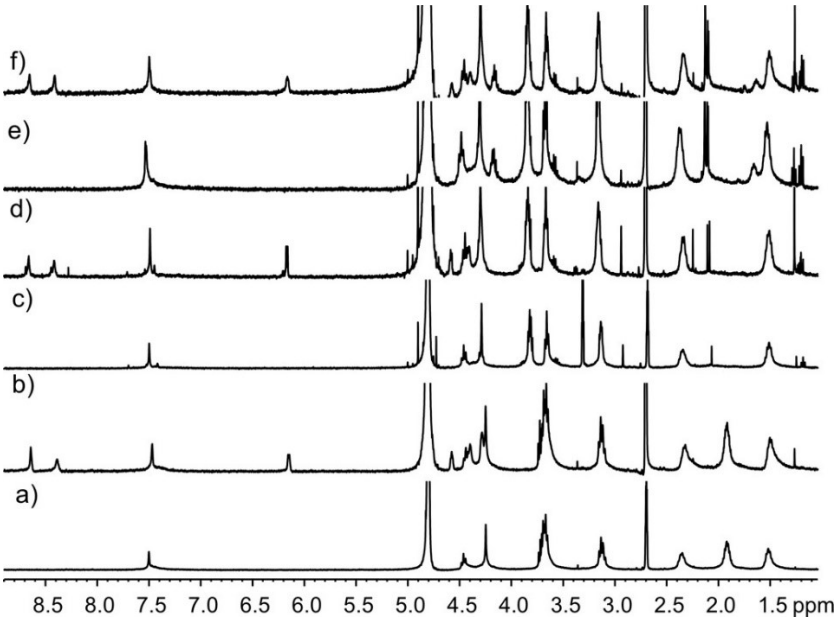

Figure S39. ^{1}H NMR spectra (D_2O/[D_6]DMSO 9/1 v/v, 298 K) of the pure host: (a) C3OHNARCl_4, (c) C3OHNARBr_4, (e) C3OHNAROTf_4, and equimolar mixtures of (b) ATP@C3OHNAR$(Cl)_4$, (b) ATP@C3OHNAR$(Br)_4$, (b) ATP@C3OHNAR$(OTf)_4$. The displaced anions are represented in parentheses. Star represents the residual D_2O solvent. The dash lines give an indication of the signal changes in ppm.

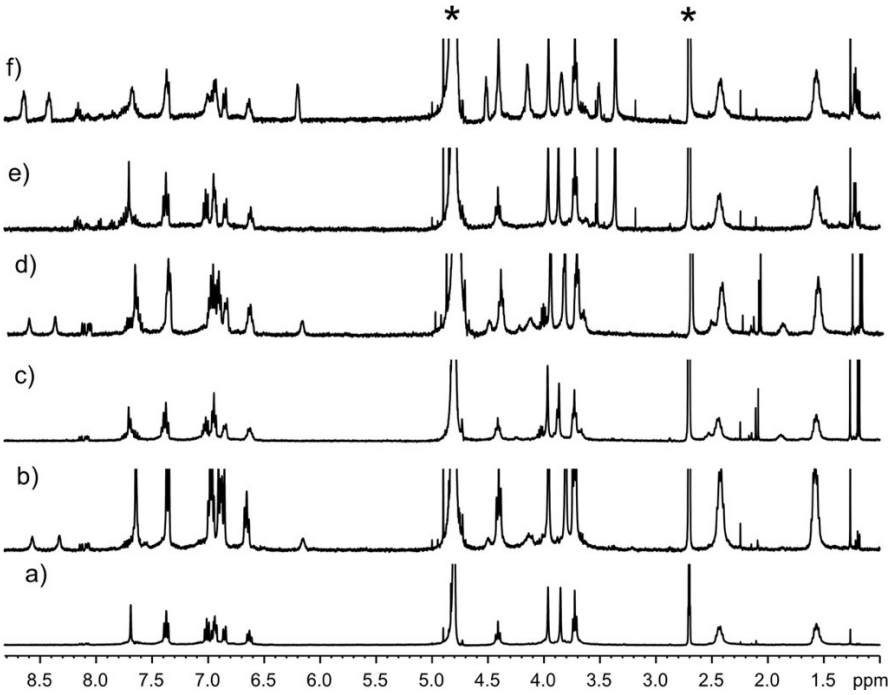

Figure S40. ^{1}H NMR spectra (D_2O/[D_6]DMSO 9/1 v/v, 298 K) of the pure host: (a) NpNARCl_4, (c) NpNARBr_4, (e) NpNAROTf_4, and equimolar mixtures of (b) AMP@NpNAR$(Cl)_4$, (b) AMP@NpNAR$(Br)_4$, (b) AMP@NpNAR$(OTf)_4$. The displaced anions are represented in parentheses. Star represents the residual D_2O solvent. The dash lines give an indication of the signal changes in ppm.

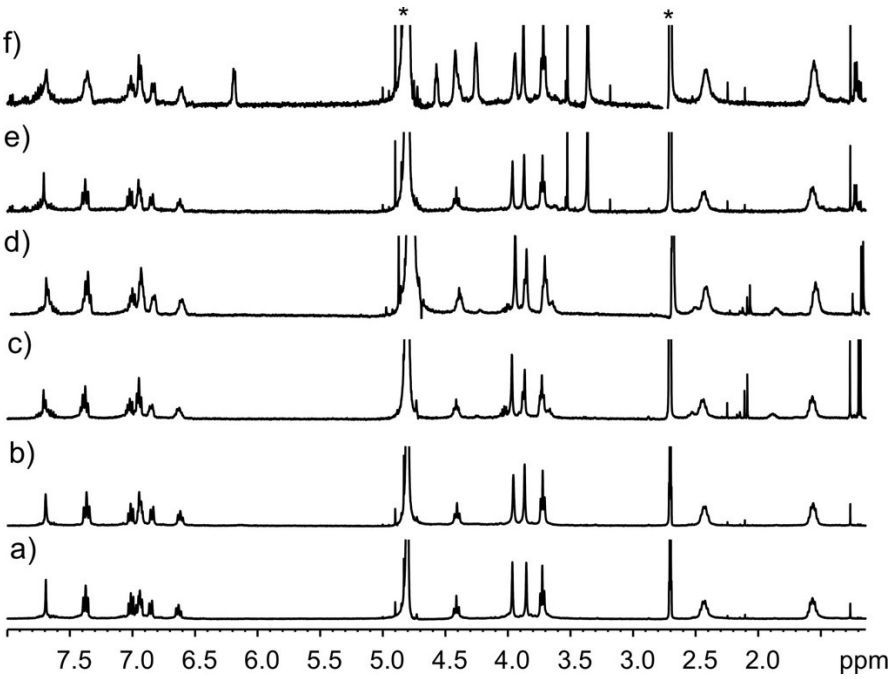

Figure S41. ^{1}H NMR spectra (D_2O/[D_6]DMSO 9/1 v/v, 298 K) of the pure host: (a) $NpNARCl_4$, (c) $NpNARBr_4$, (e) $NpNAROTf_4$, and equimolar mixtures of (b) ADP@$NpNAR(Cl)_4$, (b) ADP@$NpNAR(Br)_4$, (b) ADP@$NpNAR(OTf)_4$. The displaced anions are represented in parentheses. Star represents the residual D_2O solvent. The dash lines give an indication of the signal changes in ppm.

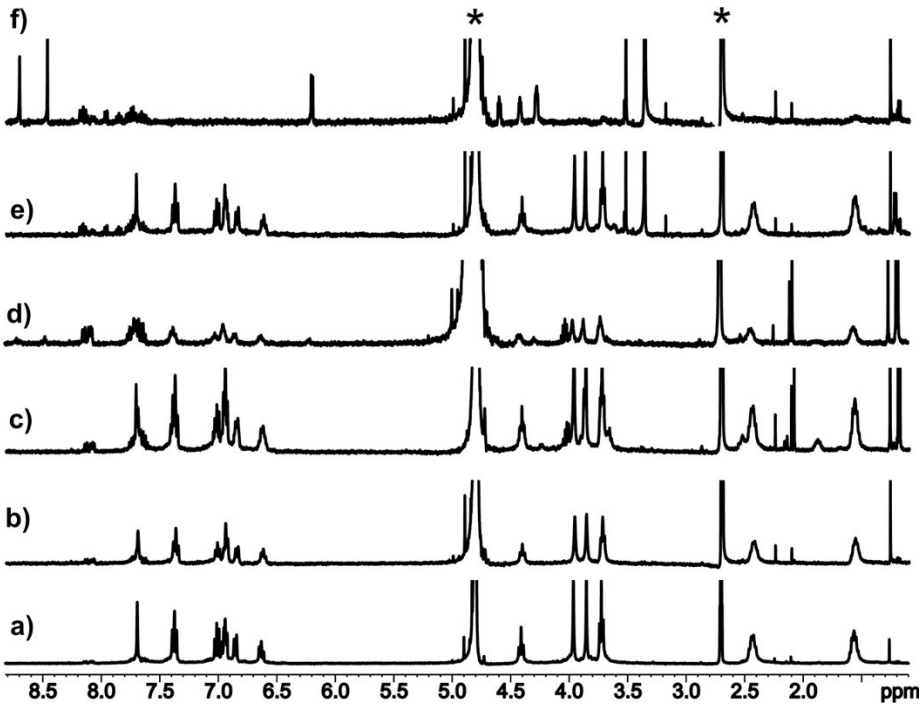

Figure S42. ^{1}H NMR spectra (D_2O/[D_6]DMSO 9/1 v/v, 298 K) of the pure host: (a) $NpNARCl_4$, (c) $NpNARBr_4$, (e) $NpNAROTf_4$, and equimolar mixtures of (b) ATP@$NpNAR(Cl)_4$, (b) ATP@$NpNAR(Br)_4$, (b) ATP@$NpNAR(OTf)_4$. The displaced anions are represented in parentheses. Star represents the residual D_2O solvent. The dash lines give an indication of the signal changes in ppm.

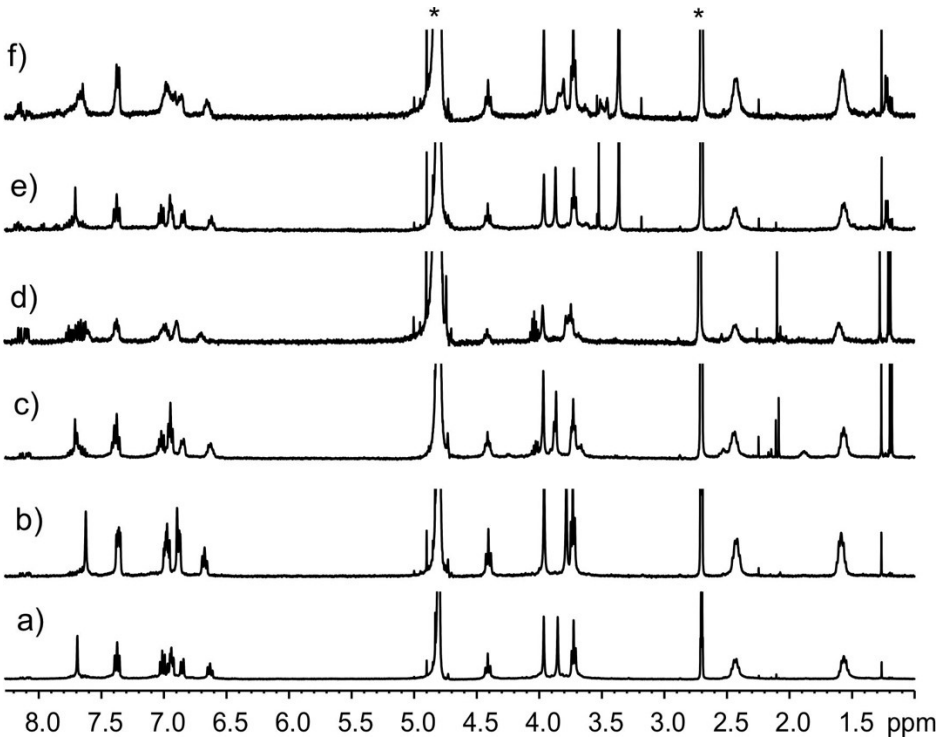

Figure S43. ^{1}H NMR spectra (D_2O/[D_6]DMSO 9/1 v/v, 298 K) of the pure host: (a) $NpNARCl_4$, (c) $NpNARBr_4$, (e) $NpNAROTf_4$, and equimolar mixtures of (b) PO_4^{3-}@$NpNAR(Cl)_4$, (b) PO_4^{3-}@$NpNAR(Br)_4$, (b) PO_4^{3-}@$NpNAR(OTf)_4$. The displaced anions are represented in parentheses. Star represents the residual D_2O solvent. The dash lines give an indication of the signal changes in ppm.

a) ^{31}P-NMR Spectra

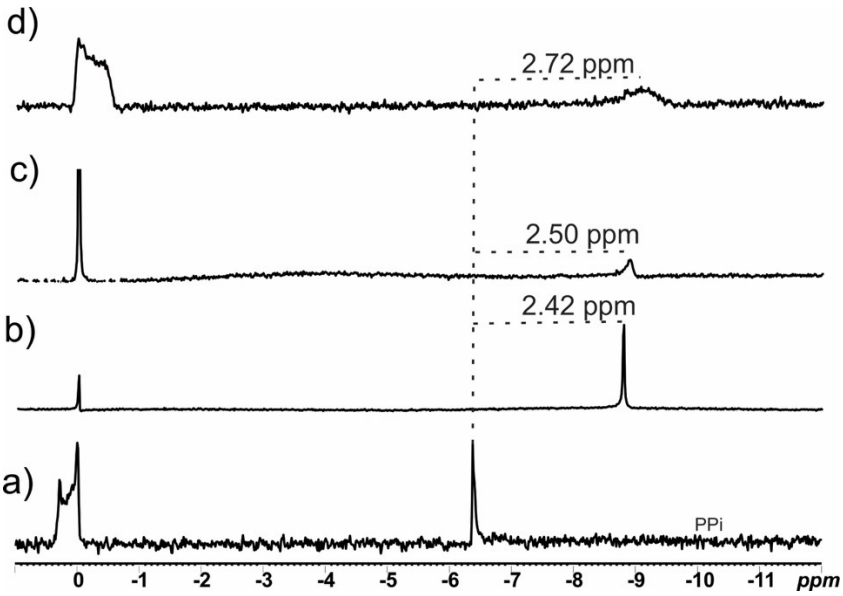

Figure S44. ^{31}P NMR spectra (D_2O/[D_6]DMSO 9/1 v/v, 298 K) of (a) PPi, and equimolar mixtures of (b) PPi@$NpNAR(Cl)_4$, (c) PPi@$NpNAR(Br)_4$ and (d) PPi@$NpNAR(OTf)_4$. The displaced anions are represented in parentheses. The dash lines give an indication of the signal changes in ppm.

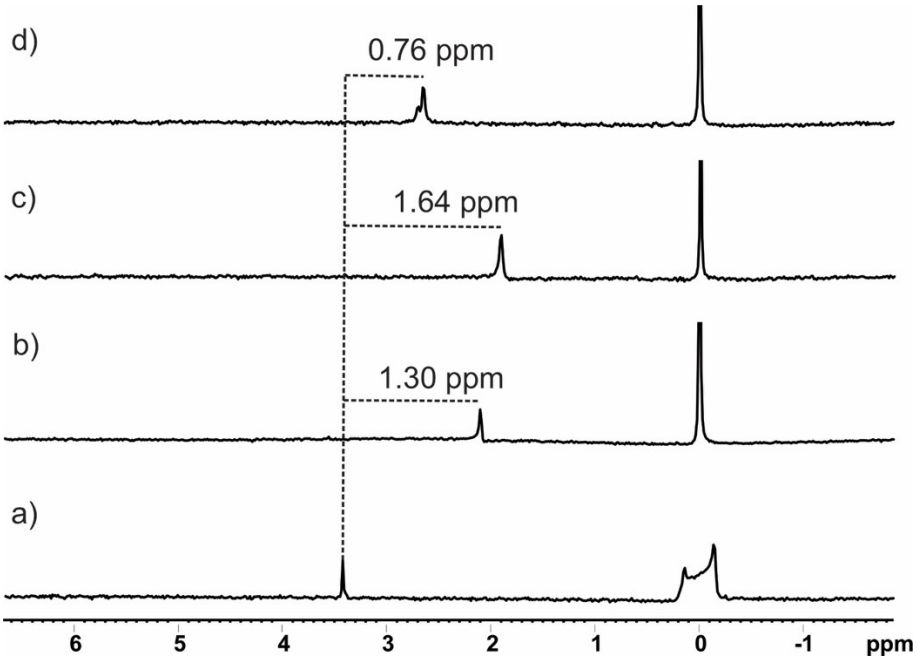

Figure S45. ^{31}P NMR spectra (D_2O/[D_6]DMSO 9/1 v/v, 298 K) of (a) PO_4^{3-}, and equimolar mixtures of (b) PO_4^{3-}@C3OHNAR(Cl)$_4$, (c) PO_4^{3-}@C3OHNAR(Br)$_4$ and (d) PO_4^{3-}@C3OHNAR(OTf)$_4$. The displaced anions are represented in parentheses. The dash lines give an indication of the signal changes in ppm.

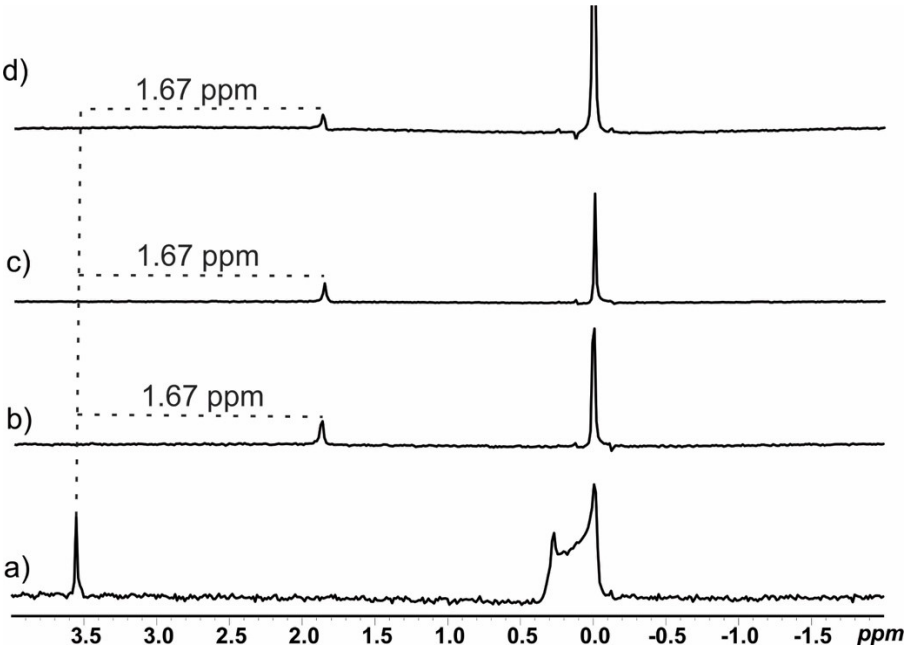

Figure S46. ^{31}P NMR spectra (D_2O/[D_6]DMSO 9/1 v/v, 298 K) of (a) PO_4^{3-}, and equimolar mixtures of (b) PO_4^{3-}@NpNAR(Cl)$_4$, (c) PO_4^{3-}@NpNAR(Br)$_4$ and (d) PO_4^{3-}@NpNAR(OTf)$_4$. The displaced anions are represented in parentheses. The dash lines give an indication of the signal changes in ppm.

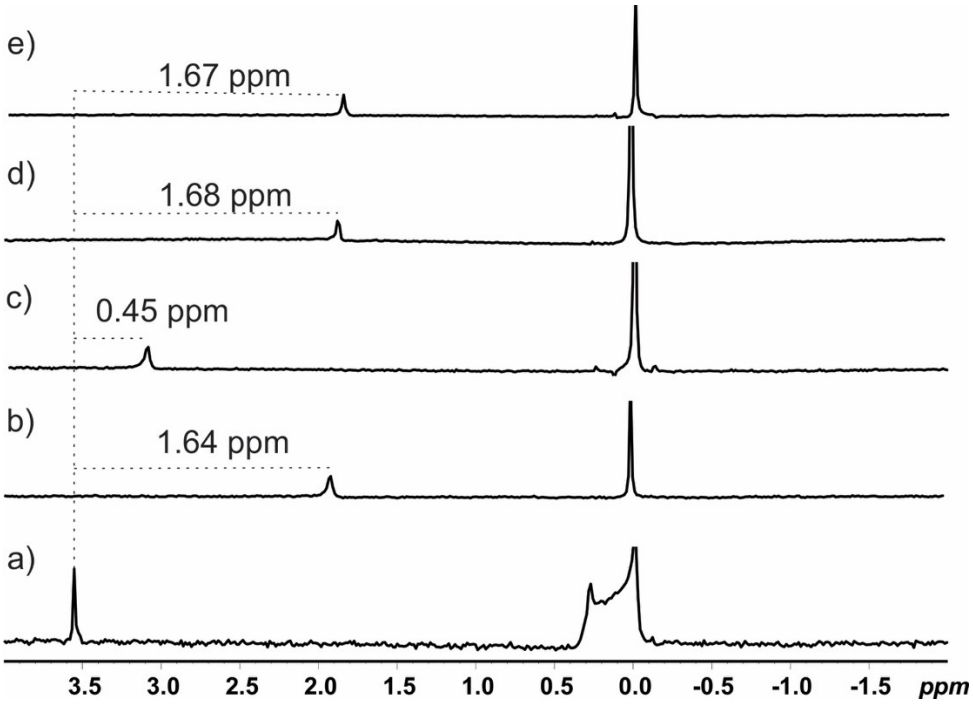

Figure S47. ^{31}P NMR spectra (D_2O/[D_6]DMSO 9/1 v/v, 298 K) of (a) PO_4^{3-}, and equimolar mixtures of (b) PO_4^{3-}@C3OHNAR(Br)$_4$, (c) PO_4^{3-}@CyNAR(Br)$_4$, (d) PO_4^{3-}@BnNAR(Br)$_4$ and (e) PO_4^{3-}@NpNAR(Br)$_4$. The displaced anions are represented in parentheses. The dash lines give an indication of the signal changes in ppm.

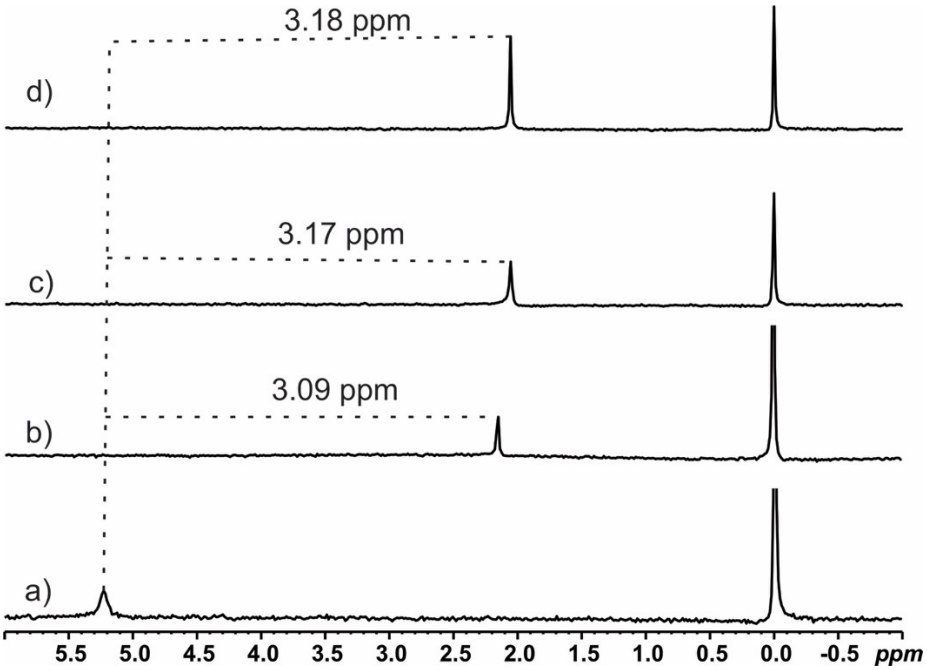

Figure S48. ^{31}P NMR spectra (D_2O/[D_6]DMSO 9/1 v/v, 298 K) of (a) AMP, and equimolar mixtures of AMP@C3OHNAR(Cl)$_4$, (c) AMP@C3OHNAR(Br)$_4$ and (d) AMP@C3OHNAR(OTf)$_4$. The displaced anions are represented in parentheses. The dash lines give an indication of the signal changes in ppm.

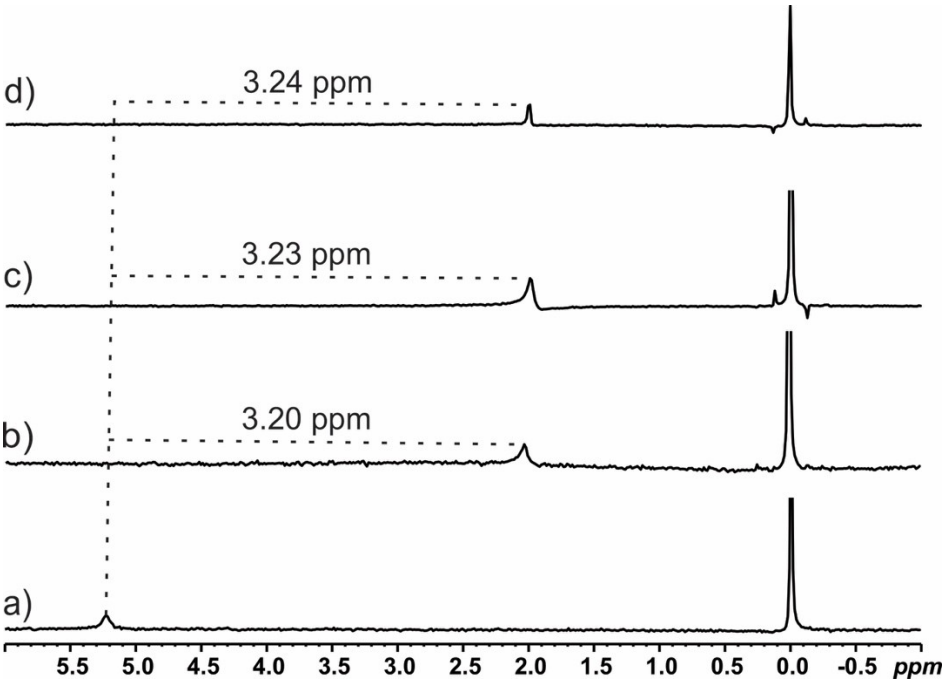

Figure S49. ^{31}P NMR spectra (D_2O/[D_6]DMSO 9/1 v/v, 298 K) of (a) AMP, and equimolar mixtures of (b) AMP@NpNAR(Cl)$_4$, (c) AMP@NpNAR(Br)$_4$ and (d) AMP@NpNAR(OTf)$_4$. The displaced anions are represented in parentheses. The dash lines give an indication of the signal changes in ppm.

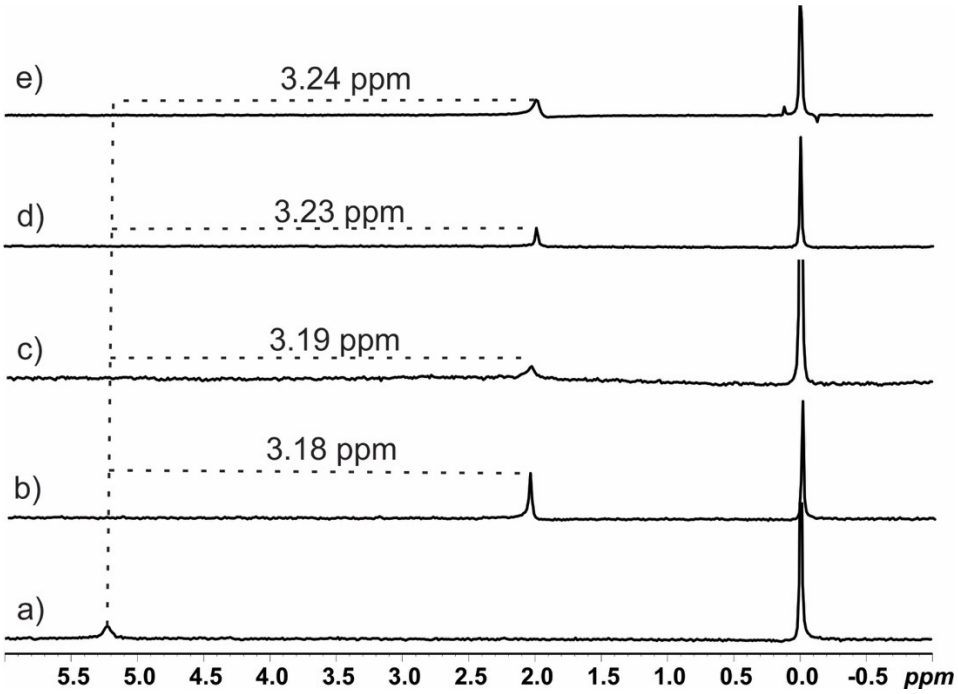

Figure S50. ^{31}P NMR spectra (D_2O/[D_6]DMSO 9/1 v/v, 298 K) of (a) AMP, and equimolar mixtures of (b) AMP@C3OHNAR(Br)$_4$, (c) AMP@CyNAR(Br)$_4$, (d) AMP@BnNAR(Br)$_4$ and (e) AMP@NpNAR(Br)$_4$. The displaced anions are represented in parentheses. The dash lines give an indication of the signal changes in ppm.

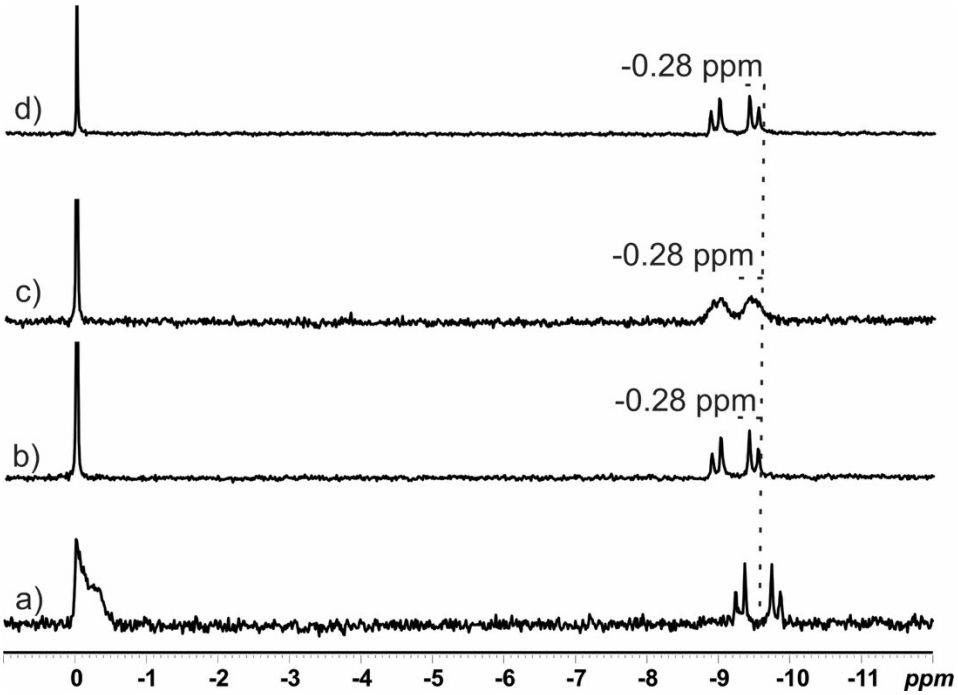

Figure S51. ^{31}P NMR spectra (D_2O/[D_6]DMSO 9/1 v/v, 298 K) of (a) ADP, and equimolar mixtures of ADP@C3OHNAR(Cl)$_4$, (c) ADP@C3OHNAR(Br)$_4$ and (d) ADP@C3OHNAR(OTf)$_4$. The displaced anions are represented in parentheses. The dash lines give an indication of the signal changes in ppm.

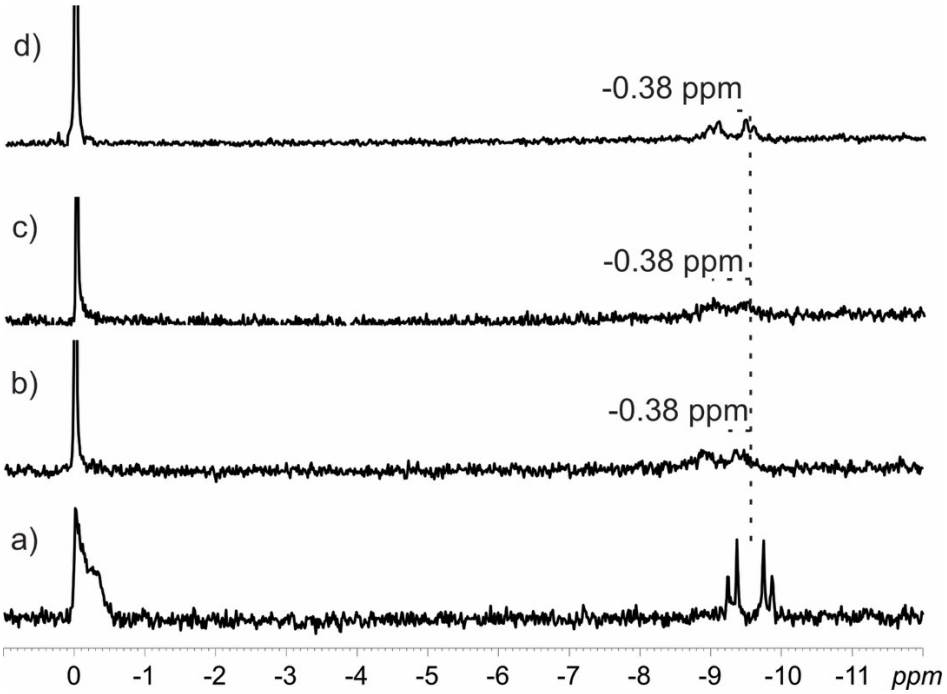

Figure S52. ^{31}P NMR spectra (D_2O/[D_6]DMSO 9/1 v/v, 298 K) of (a) ADP, and equimolar mixtures of (b) ADP@NpNAR(Cl)$_4$, (c) ADP@NpNAR(Br)$_4$ and (d) ADP@NpNAR(OTf)$_4$. The displaced anions are represented in parentheses. The dash lines give an indication of the signal changes in ppm.

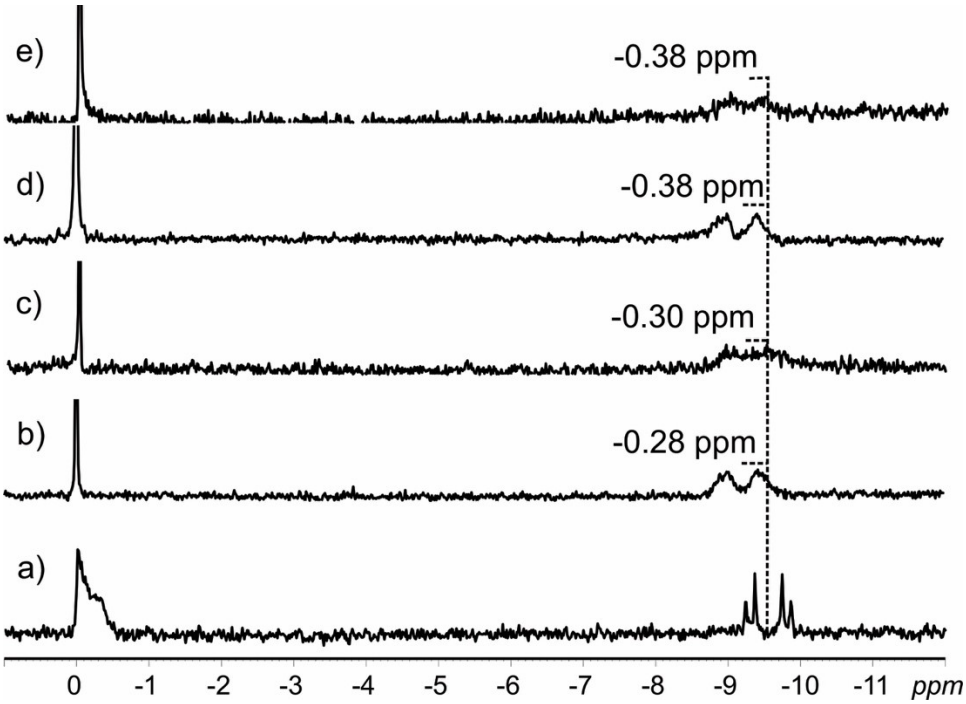

Figure S53. ^{31}P NMR spectra (D_2O/[D_6]DMSO 9/1 v/v, 298 K) of (a) AMP, and equimolar mixtures of (b) ADP@C3OHNAR(Br)$_4$, (c) ADP@CyNAR(Br)$_4$, (d) ADP@BnNAR(Br)$_4$ and (e) ADP@NpNAR(Br)$_4$. The displaced anions are represented in parentheses. The dash lines give an indication of the signal changes in ppm.

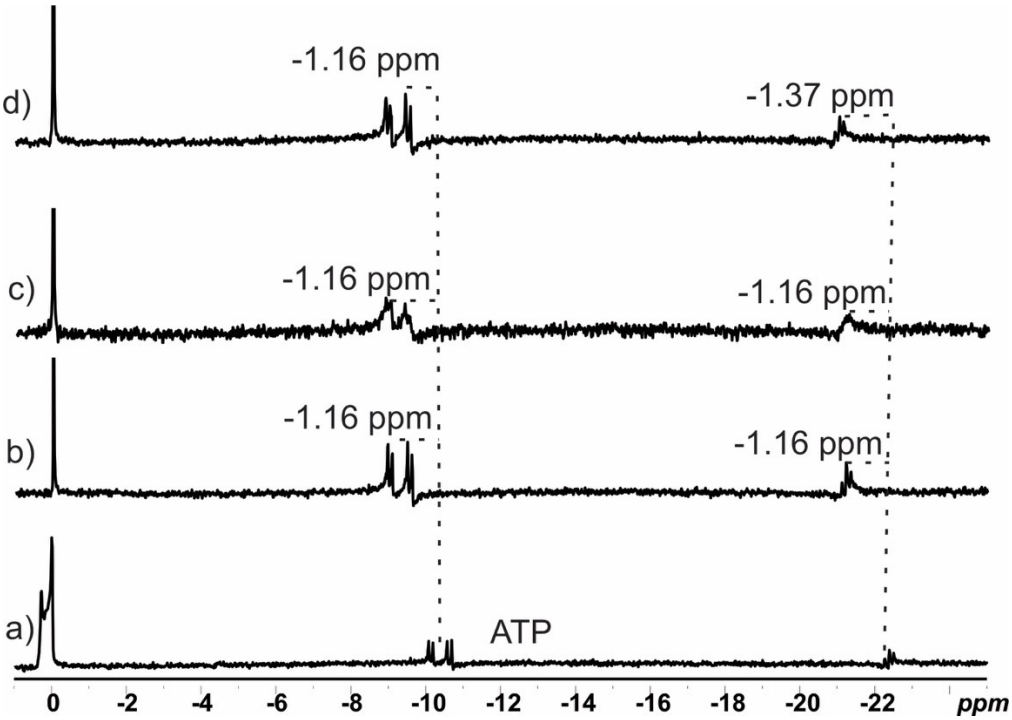

Figure S54. ^{31}P NMR spectra (D_2O/[D_6]DMSO 9/1 v/v, 298 K) of (a) ATP, and equimolar mixtures of ATP@C3OHNAR(Cl)$_4$, (c) ATP@C3OHNAR(Br)$_4$ and (d) ATP@C3OHNAR(OTf)$_4$. The displaced anions are represented in parentheses. The dash lines give an indication of the signal changes in ppm.

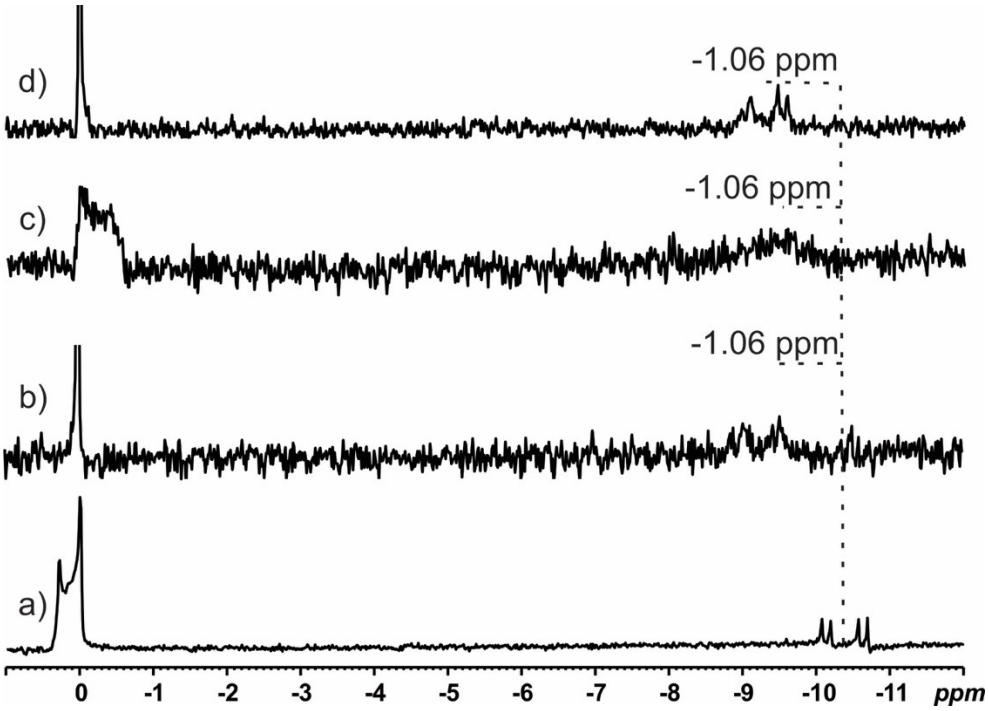

Figure S55. ^{31}P NMR spectra (D_2O/[D_6]DMSO 9/1 v/v, 298 K) of (a) ATP, and equimolar mixtures of (b) ATP@NpNAR(Cl)$_4$, (c) ATP@NpNAR(Br)$_4$ and (d) ATP@NpNAR(OTf)$_4$. The displaced anions are represented in parentheses. The dash lines give an indication of the signal changes in ppm.

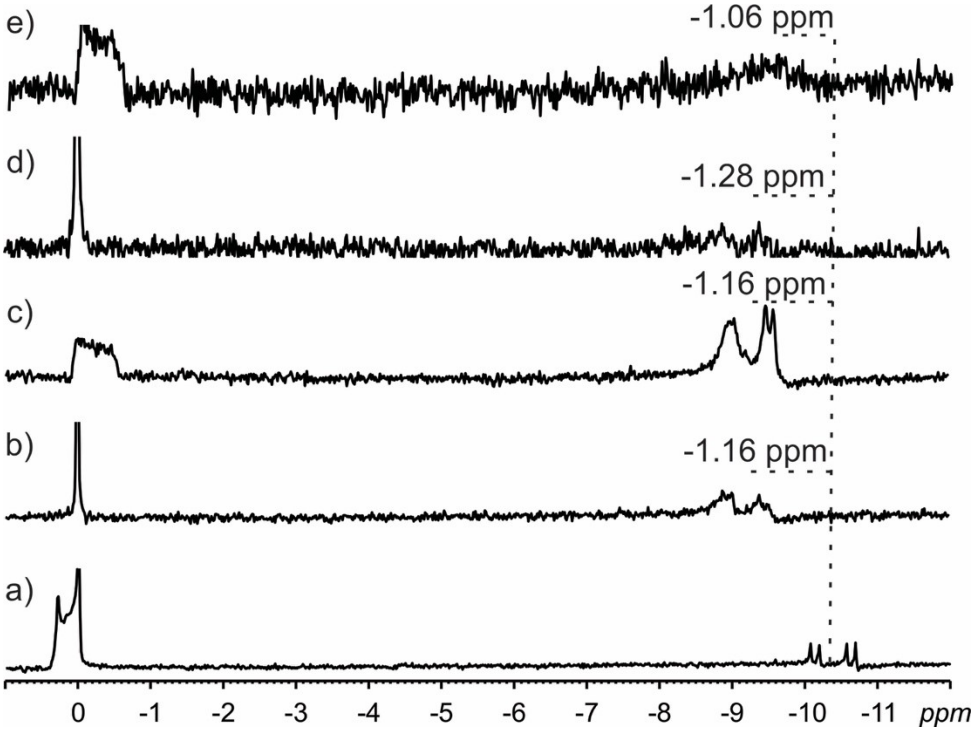

Figure S56. ^{31}P NMR spectra (D_2O/[D_6]DMSO 9/1 v/v, 298 K) of (a) ATP, and equimolar mixtures of (b) ATP@C3OHNAR(Br)$_4$, (c) ATP@CyNAR(Br)$_4$, (d) ATP@BnNAR(Br)$_4$ and (e) ATP@NpNAR(Br)$_4$. The displaced anions are represented in parentheses. The dash lines give an indication of the signal changes in ppm.

5. COMPUTATIONAL MODELLING

All structures were calculated using the Gaussian 09 suite of programs[6] applying at the ωB97X-D[6]/6-311-G(d,p) level of theory and SCRF=SMD solvation model using generic keyword to consider a solvation cluster of 1DMSO:9H_2O (according to experimental concentration) for solvent effects. To further validated both long-ranged and short-ranged interactions within the systems, the single point calculations were done using the dispersion-corrected functional (B39W91) which is appropriate for modelling the H-bonding and dispersive non-covalent host–guest interactions. Structure visualization was performed using GaussView v5.0.8.4 and Maestro 11.[7]

We evaluated the change in Gibbs free energy (ΔG) for binding event, as

$$\mathbf{\Delta G = BE + \Delta E_{zpe} + T\Delta S + \Delta PV}$$

The BE can be determined directly by analyzing the DFT total energies:

$$\mathbf{\Delta G = BE + \Delta E_{zpe} + T\Delta S + \Delta PV = [E_{complex} - (E_H + E_G)] + [Ezpe_{complex} - (E_H + E_G)] + T [S_{complex} - (S_H + S_G)]}$$

where Ecomplex, EH, and EG are the DFT total energies of the complex, free host, and guest, respectively. **Δ**Ezpe and **Δ**S are the zero-point energy difference and the entropy difference between the complex and reactants, respectively.

To obtain insights into the dynamical behavior of the counteranion at the molecular level, a molecular dynamics (MD) study was performed for the complexation of the Np-host with the OTf anions using the OPLS-2005 force field using the disordered system approach of Desmond[8] to build a solvation cluster of 1DMSO:9H_2O (according to experimental concentration) enveloping the host-guest complex (the solute) consisting of 2NpNAR4+ system plus 8OTf- counterions in the box of co-mixture of 400DMSO:1200H_2O molecules. The energy of the system was further minimized with 1000 steps of steepest descent followed by 3500 steps of conjugate gradient minimization. The molecular dynamics simulations started with a 1 fs integration time step; the complex structure was then relaxed for 10 ps. The temperature of the relaxed system was equilibrated at 300K via 5 and 0 ns of MD by 2 fs time steps using the Langevin dynamics applying a collision frequency of 10 ps^{-1} with a velocity limit of 5 temperature units. The generated coordinates after were then applied to do 5 ns followed by 10 ns and 20 ns molecular dynamics using 2 fs time steps, with temperature being fixed at 300 K applying the Langevin dynamics a collision frequency of 1 ps^{-1} and a velocity limit of 20 temperature units. The pressure of the solvated system was then equilibrated at 1 bar at a specified density in a constant pressure periodic boundary applying an isotropic pressure scaling method using a pressure relaxation time of 2 ps with the time step of the 2 fs with a cut-off of 9 Å for the non-bonded interaction.

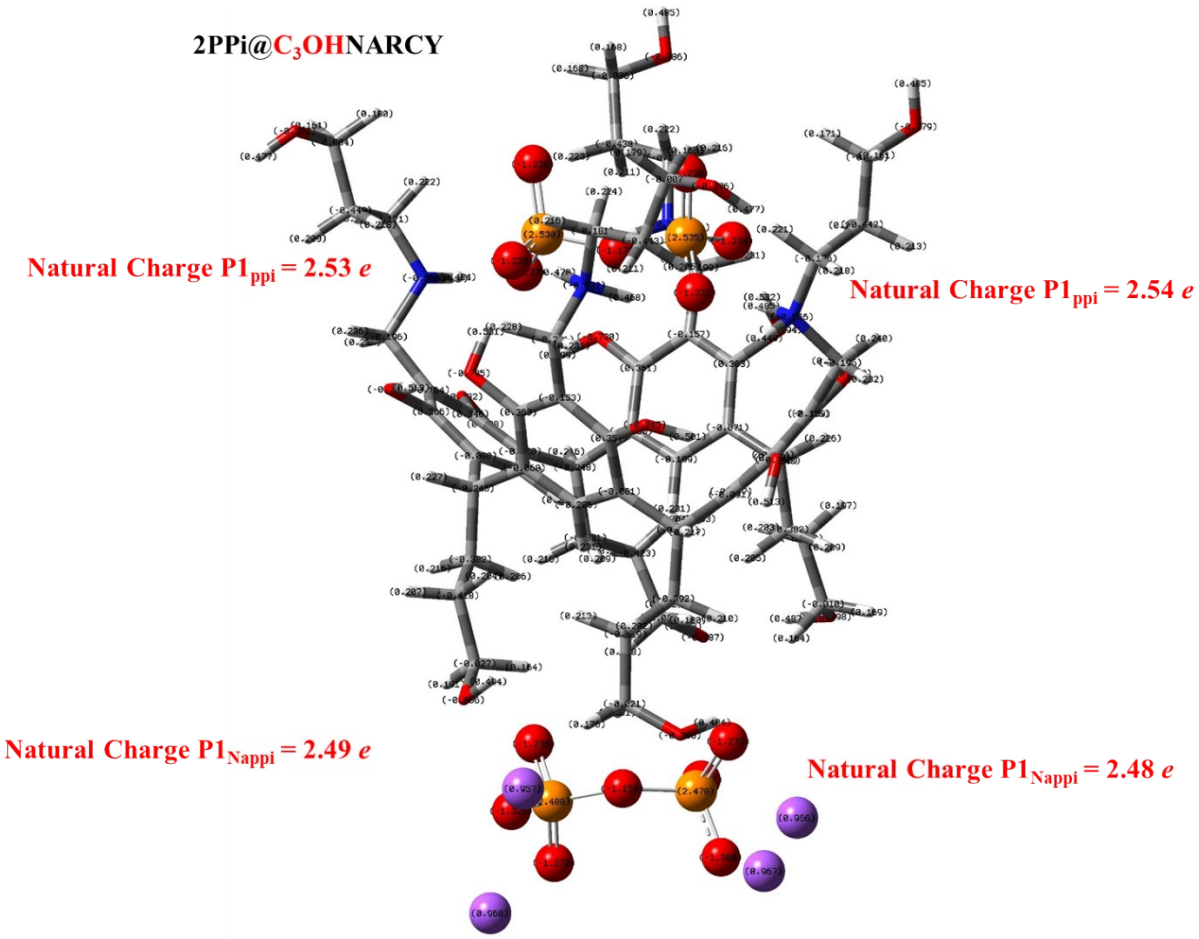

Figure S57. The calculated Natural charge density (obtained by NBO analysis) on each atom in the **2PPi@C3OHNARCY** complex. The higher electron density on the phosphorous atoms in the cavity would be reflected in a greater upfield shift in their resonances. The near symmetry of the system leads to each pair of phosphorous atoms having almost the same charge density.

Thermodynamic Data

C3OHNAR(Cl)$_4$

```
# opt=calcfc freq=noraman wb97xd/6-311g(d,p) scrf=(solvent=generic,rea
 d,smd) nosymm 5d temperature=298
Zero-point correction=                           1.465575
(Hartree/Particle)
 Thermal correction to Energy=                    1.552187
 Thermal correction to Enthalpy=                  1.553131
 Thermal correction to Gibbs Free Energy=         1.339647
 Sum of electronic and zero-point Energies=          -5449.315358
 Sum of electronic and thermal Energies=             -5449.228746
 Sum of electronic and thermal Enthalpies=           -5449.227802
 Sum of electronic and thermal Free Energies=        -5449.441286
```

C3OHNAR(OTf)$_4$

```
# opt=calcfc freq=noraman wb97xd/6-311g(d,p) scrf=(solvent=generic,rea
 d,smd) 5d temperature=298
 ---------------------------------------------------------------------
-Zero-point correction=                           1.580996
(Hartree/Particle)
 Thermal correction to Energy=                    1.695820
 Thermal correction to Enthalpy=                  1.696764
 Thermal correction to Gibbs Free Energy=         1.419059
 Sum of electronic and zero-point Energies=          -7454.339054
 Sum of electronic and thermal Energies=             -7454.224230
 Sum of electronic and thermal Enthalpies=           -7454.223287
 Sum of electronic and thermal Free Energies=        -7454.500991
```

NpNAR(Cl)$_4$

```
# opt=calcfc freq=noraman wb97xd/6-311g(d,p) scrf=(solvent=generic,rea
 d,smd) 5d temperature=298
Zero-point correction=                           1.737478
(Hartree/Particle)
 Thermal correction to Energy=                    1.835067
 Thermal correction to Enthalpy=                  1.836011
 Thermal correction to Gibbs Free Energy=         1.602751
 Sum of electronic and zero-point Energies=          -6371.991672
 Sum of electronic and thermal Energies=             -6371.894083
 Sum of electronic and thermal Enthalpies=           -6371.893140
 Sum of electronic and thermal Free Energies=        -6372.126400
```

PPi@C3OHNAR

```
# opt=calcfc freq=noraman wb97xd/6-311g(d,p) scrf=(solvent=generic,rea
 d,smd) nosymm 5d temperature=298
```

```
Zero-point correction=                           1.496575
(Hartree/Particle)
 Thermal correction to Energy=                    1.582116
 Thermal correction to Enthalpy=                  1.583059
 Thermal correction to Gibbs Free Energy=         1.379358
 Sum of electronic and zero-point Energies=          -4817.926247
 Sum of electronic and thermal Energies=             -4817.840706
 Sum of electronic and thermal Enthalpies=           -4817.839762
 Sum of electronic and thermal Free Energies=        -4818.043463
```

PPi@NpNAR

```
# opt=calcfc freq=noraman wb97xd/6-311g(d,p) scrf=(solvent=generic,rea
 d,smd) nosymm 5d temperature=298
Zero-point correction=                           1.763045
(Hartree/Particle)
 Thermal correction to Energy=                    1.861000
 Thermal correction to Enthalpy=                  1.861944
 Thermal correction to Gibbs Free Energy=         1.634207
 Sum of electronic and zero-point Energies=          -5740.604973
 Sum of electronic and thermal Energies=             -5740.507018
 Sum of electronic and thermal Enthalpies=           -5740.506074
 Sum of electronic and thermal Free Energies=        -5740.733812
```

2PPi@C3OHNAR

```
# opt=calcfc freq=noraman wb97xd/6-311g(d,p)
scrf=(solvent=generic,read,smd) geom=connectivity 5d temperature=298
Zero-point correction=                           1.531757
(Hartree/Particle)
Thermal correction to Energy=                    1.634988
Thermal correction to Enthalpy=                  1.635932
Thermal correction to Gibbs Free Energy=         1.390701
Sum of electronic and zero-point Energies=          -6676.997482
Sum of electronic and thermal Energies=             -6676.894252
Sum of electronic and thermal Enthalpies=           -6676.893308
Sum of electronic and thermal Free Energies=        -6677.138539
```

2PPi@NpNAR

```
# opt=calcfc freq=noraman wb97xd/6-311g(d,p)
scrf=(solvent=generic,read,smd) nosymm 5d temperature=298
Zero-point correction=                           1.799290
(Hartree/Particle)
Thermal correction to Energy=                    1.913218
Thermal correction to Enthalpy=                  1.914162
Thermal correction to Gibbs Free Energy=         1.650245
Sum of electronic and zero-point Energies=          -7599.688795
Sum of electronic and thermal Energies=             -7599.574867
Sum of electronic and thermal Enthalpies=           -7599.573923
```

Sum of electronic and thermal Free Energies= -7599.837840

6. REFERENCES

1. N. K. Beyeh, I. Díez, S. M. Taimoory, D. Meister, A. I. Feig, J. F. Trant, R. H. A. Ras and K. Rissanen, *Chem. Sci.*, **2018**, 9, 1358–1367.
2. N. K. Beyeh, H. H. Jo, I. Kolesnichenko, F. Pan, E. Kalenius, E. v. Anslyn, R. H. A. Ras and K. Rissanen, *J. Org. Chem.*, **2017**, 82, 5198–5203.
3. N. K. Beyeh, M. Cetina, M. Lofman, M. Luostarinen, A. Shivanyuk and K. Rissanen, *Supramol. Chem.*, **2010**, 22, 737–750.
4. A. Shivanyuk, T. P. Spaniol, K. Rissanen, E. Kolehmainen and V. Böhmer, *Angew. Chem.*, **2000**, 39, 3497–3500.
5. K. A. Connors, *Binding constants: the measurement of molecular complex stability*, Wiley, **1987**.
6. Frisch, M. J.; Trucks, G. W.; Schlegel, H. B.; Scuseria, G. E.; Robb, M. A.; Cheeseman, J. R.; Scalmani, G.; Barone, V.; Mennucci, B.; Petersson, G. A.; Nakatsuji, H.; Caricato, M.; Li, X.; Hratchian, H. P.; Izmaylov, A. F.; Bloino, J.; Zhang, G.; Sonnenberg, J. L.; Hada, M.; Ehara, M.; Toyota, K.; Fukuda, R.; Hasegawa, J.; Ishida, M.; Nakajima, T.; Honda, Y.; Kitao, O.; Nakai, H.; Vreven, T.; Montgomery, J. A.; Peralta, Jr., J. E.; Ogliaro, F.; Bearpark, M.; Heyd, J. J.; Brothers, E.; Kudin, K. N.; Staroverov, V. N.; Kobayashi, R.; Normand, J.; Raghavachari, K.; Rendell, A.; Burant, J. C.; Iyengar, S. S.; Tomasi, J.; Cossi, M.; Rega, N.; Millam, J. M.; Klene, M.; Knox, J.e.; Cross, J. B.; Bakken, V.; Adamo, C.; Jaramillo, J.; Gomperts, R.; Stratmann, R. E.; Yazyev, O.; Austin, A. J.; Cammi, A. R.; Pomelli, C.; Ochterski, J. W.; Martin, R. L.; Morokuma, K.; Zakrzewski, V. G.; Voth, G. A.; Salvador, P.; Dannenberg, J. J.; Dapprich, S.; Daniels, A. D.; Farkas, Ö.; Foresman, J. B.; Ortiz, J. V.; Cioslowski, J.; Fox, D. J.*Gaussian 09, Revision C.02*; Gaussian, Inc.: Wallingford, CT, **2009**.
7. J. da Chai and M. Head-Gordon, *Phys. Chem. Chem. Phys.*, **2008**, 10, 6615–6620.
8. Molecular Dynamics System, D. E. Shaw Research, New York, NY, 2021. Maestro-Desmond Interoperability Tools, Schrödinger, New York, NY, **2021**.